Generalized Voltage-Based State-Space Modeling of Modular Multilevel Converters With Constant Equilibrium in Steady State

Gilbert Bergna-Diaz , Julian Freytes , Xavier Guillaud, *Member, IEEE*, Salvatore D'Arco, and Jon Are Suul , *Member, IEEE*

Abstract—This paper demonstrates that the sum and difference of the upper and lower arm voltages are suitable variables for deriving a generalized state-space model of a modular multilevel converter (MMC) which settles at a constant equilibrium in steady-state operation. The presented modeling approach separates the multiple frequency components appearing within the MMC as a first step of the model derivation, to avoid variables containing multiple frequency components in steady state. On this basis, it is shown that Park transformations at three different frequencies ($+\omega$, -2ω, and $+3\omega$) can be applied for deriving a model formulation where all state-variables settle at constant values in steady state, corresponding to an equilibrium point of the model. The resulting model accurately captures the internal current and voltage dynamics and the coupling between the different frequency components appearing in the variables of a three-phase MMC. Independently of the control system implementation, the derived equations are valid for accurate representation of the MMC in the applied dqz reference frames, and they can be linearized for utilization in eigenvalue-based analysis of small-signal dynamics. Furthermore, the model can be utilized for control system design by multivariable methods requiring any stable equilibrium to be defined by a fixed operating point. Time-domain simulations in comparison to an established average model of the MMC, as well as results from a detailed simulation model of an MMC with 400 submodules per arm, are presented as verification of the validity and accuracy of the developed model.

Index Terms—HVDC transmission, modular multilevel converter (MMC), Park transformations, state-space modeling.

I. Introduction

THE modular multilevel converter (MMC) is emerging as the preferred topology for voltage source converter (VSC)-based HVDC transmission schemes [1], [2]. Especially in terms of its low losses, modularity, scalability, and low harmonic content in the output ac voltage, the MMC topology provides significant advantages for HVDC applications compared to two- or three-level VSCs. However, the MMC is characterized by additional internal dynamics related to the circulating currents and the internal capacitor voltages of the upper and lower arms of each phase [3], [4]. Thus, the modeling, control, and analysis of the MMC is more complicated than for other VSC topologies.

Different types of studies are necessary for design and analysis of MMC-based HVDC transmission systems, requiring various detailing levels in the modeling. A general overview of MMC modeling approaches suitable for different types of studies is shown in Fig. 1. The most detailed models can simulate the switching operations of the individual submodules (SMs) of the MMC, as indicated to the left of the figure. Such models can be used for studying all modes of operation and all the control loops of the MMC, including the algorithms for balancing the SM voltages. If equal voltage distribution among the SMs in each arm of an MMC can be assumed, arm averaged models (AAM) can be introduced. An AAM implies that each arm of the MMC can be represented by a controllable voltage source associated with a corresponding equivalent capacitance, and introduces a significant reduction of complexity while still maintaining an accurate representation of the internal dynamics [3]–[6]. Thus, AAM models, or equivalent energy-based models, are suitable for simplified simulations and analysis of MMCs, and are widely used as basis for control system design [4], [6], [7].

A. State-Space Modeling of MMCs

When considering multivariable systems with coupled dynamics, state-space modeling can be a flexible framework for simulation and analysis [8]. Thus, various state-space models of MMCs have been presented in the literature, including switching cycle models [9] and continuous time average models based on the AAM approach [5], [10]–[14]. Some
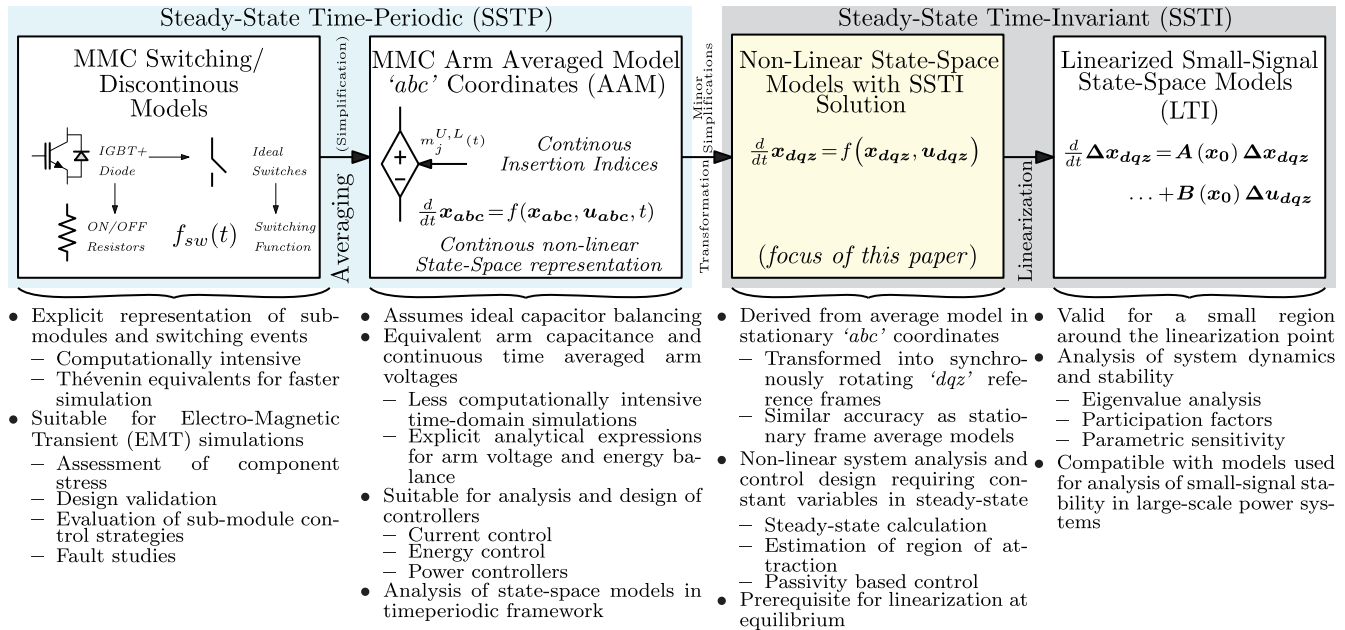
Fig. 1.   Overview of MMC modeling approaches and their areas of application.

of the developed state-space models have also been utilized for applying linear quadratic regulator (LQR) strategies, as discussed in [11], [12], [15], and [16]. However, the state-space representation used in [11], [12], and [15] are simplified models that do not represent all the internal dynamics of the MMC, while the model used in [16] represents the MMC by steady-state time-periodic (SSTP) state variables.

Models with SSTP characteristics imply that steady-state operation is characterized by an orbit and not by an equilibrium point of the state variables. Furthermore, the currents and capacitor voltages in each arm of the MMC contain multiple frequency components [17]. This prevents straightforward application of the Park transformation for obtaining state-space models of three-phase MMCs represented in a single synchronously rotating reference frame (SRRF) according to the modeling approaches commonly applied for control system design and small-signal stability analysis of two-level VSCs [18]–[20]. Indeed, SSTP state-space models cannot be directly used for system-oriented stability analysis based on traditional eigenvalue techniques as commonly applied in studies of power system stability. Instead, stability analysis of such models will require advanced methods specifically developed for time-periodic systems, as recently studied in [21].

Obtaining a linearizable state-space model that can be utilized by traditional techniques for eigenvalue-based stability analysis requires a model formulation with a uniquely defined equilibrium point for each operating condition, which corresponds to all state variables settling to constant values in steady state [22]. For an MMC, this implies that it is necessary to derive a state-space model with a steady-state time invariant (SSTI) solution in a set of suitably defined SRRFs. As indicated in the middle of Fig. 1, such an SRRF dqz model can be developed from an equivalent average model in the stationary abc coordinates. The resulting nonlinear

SSTI representation can be used for calculating the steady-state conditions corresponding to any feasible combination of input signals, and a linear time invariant (LTI) model suitable for eigenvalue analysis can be directly obtained by linearization.

B. Related Works

Several approaches for obtaining LTI state-space models of MMCs have been recently proposed in the literature, motivated by the need for representing MMC HVDC transmission systems in eigenvalue-based small-signal stability studies. The simplest approach has been to neglect parts of the internal dynamics of the MMC, and model mainly the ac-side dynamics in an SRRF together with a simplified dc-side representation, as in [23]–[25]. However, if the dynamics associated with the internal equivalent capacitor voltages of the MMC and the interaction with the circulating currents are ignored, such models will imply significant inaccuracies. Especially if a power balance between the ac- and dc-sides of the converter is assumed in the same way as for a two-level VSC model, like in [23] and [25], the model will only be suitable for representing very slow transients. Therefore, more detailed dynamic state-space models have been proposed in [26]–[32], for representing two different cases, as explained in the following.

1) The approaches presented in [26] and [27] are based on the assumption that the modulation indices for the MMC arms are calculated to compensate for the voltage oscillations in the internal equivalent arm capacitor voltage. This strategy for control system implementation is referred to as compensated modulation (CM) and limits the coupling between the internal variables of the MMC and the ac- and dc-side variables. Thus, CM-based control allows a simplified modeling of the MMC, where

only the aggregated dynamics of the zero sequence circulating current and the total energy stored in the capacitors of the MMC are represented. As a result, these models can provide accurate representation of the ac- and dc-side terminal behavior of MMCs under most conditions, but imply that the dynamics of the different oscillating components of the internal variables cannot be analyzed.

2) The approaches proposed in [28]–[30] and [32] consider all the internal variables of the MMC, under the assumption of a control system with a circulating current suppression controller (CCSC) implemented in a negative sequence double frequency SRRF [33]. Indeed, the methods proposed in [28], [29], and [32] model the MMC by representing the internal second harmonic circulating currents and the corresponding second harmonic arm voltage components in an SRRF rotating at twice the fundamental frequency. However, the harmonic superposition principles assumed in the modeling, corresponding to dynamic phasor representation, could affect the information about the nonlinear characteristics of the MMC, and correspondingly limit the applicability of the models in nonlinear techniques for analysis and control system design. A similar approximation was also made when separately modeling the fundamental frequency and the second harmonic frequency dynamics of the upper and lower arm capacitor voltages in [30].

C. Contributions

Compared to the previously published efforts on MMC modeling, the main contribution of this paper is to present a linearizable SSTI state-space representation of an MMC with as few simplifications as possible in the derivation of the model. Indeed, the proposed modeling approach is intended for preserving the fundamental nonlinearity of the stationary frame average model of the MMC that is used as a starting point for the presented derivations. This is achieved by utilizing information about how the different variables of the MMC contain mainly combinations of dc-components, fundamental frequency components, double frequency oscillations, and third harmonics, in steady-state operation. Using the sum (Σ) and difference (Δ) between the variables of the upper and lower arms of the MMC as state variables, a natural frequency separation can be obtained, where the Δ variables contain only fundamental frequency and third harmonic components while Σ variables contain only dc and 2ω components. Since the dc- and third harmonic components will be equal in all three phases, they appear only as zero sequence components. Therefore, application of appropriate Park transformations to each set of variables results in separation of the frequency components, allowing for derivation of a state-space model with SSTI solution where all variables settle to a constant equilibrium point in steady-state operation.

It should be noted that the presented nonlinear MMC model with SSTI characteristics is suitable for nonlinear control system design, for instance, by applying passivity theory [34]–[36]. However, the model can also be directly linearized to obtain a detailed small-signal model that can

be utilized for analyzing the dynamic characteristics of an MMC and its control system as well as its interaction with any ac-side or dc-side power system configuration.

The first contribution to the applied modeling approach was presented in [31], where the SSTI state equations for the internal $\Sigma-\Delta$ voltages and currents were derived for a specific implementation of the insertion index calculation. This paper extends the derivations from [31], to obtain a model that is applicable independently of the implemented strategy for calculating the modulation indices of the MMC. Furthermore, the model derivation has been expanded to include the effect of the zero sequence of the difference between upper and lower modulation indices m_z^Δ in the MMC dynamics, which was neglected in [31]. This extension of the model can be useful for representing the impact of the third harmonic injection commonly introduced for increasing the dc-voltage utilization of three phase converters [37], [38], and in case a zero sequence component in the output voltage is utilized to control the energy distribution within the MMC. The applied techniques and derivations can also be useful for SRRF modeling and analysis of MMC control strategies implemented in the stationary frame, as investigated in [39].

The modeling approach and the derivations required for obtaining the presented generalized voltage-based state-space model of an MMC with SSTI characteristics are presented in detail in the following sections. The validity of the derived model is demonstrated by time-domain simulations in comparison to the average model used as a starting point for the derivations, and the accuracy of the obtained results is verified by comparison to a detailed simulation model of an MMC with 400 SMs per arm. Furthermore, an example of linearization and small-signal analysis of the derived model is presented, demonstrating how eigenvalue-based techniques can be utilized for identifying and understanding potential small-signal stability problems within the control and operation of an MMC.

II. MMC MODELING IN THE STATIONARY FRAME

As a basis for deriving the model presented in this paper, the MMC topology is briefly recalled, and the applied $\Sigma-\Delta$ vector representation in the stationary reference frame is introduced. A simplified steady-state frequency analysis of the MMC variables is also presented as a starting point for the following derivations.

A. Average Model Representation of the MMC Topology

The basic topology of a three-phase MMC is synthesized by the series connection of N SMs with independent capacitors C to constitute one arm of the converter as indicated in Fig. 2. The SMs in one arm are connected to a filter inductor with inductance L_{arm} and equivalent resistance R_{arm} to form the connection between one of the dc-terminals and the ac-side output. Two identical arms are connected to the upper and lower dc-terminals, respectively, to form one leg for each phase j ($j = a, b, c$). The ac-side interface is assumed to be a filter inductor and/or the leakage inductance of a transformer, which is modeled by an equivalent resistance and inductance, R_f and L_f, respectively, [40].
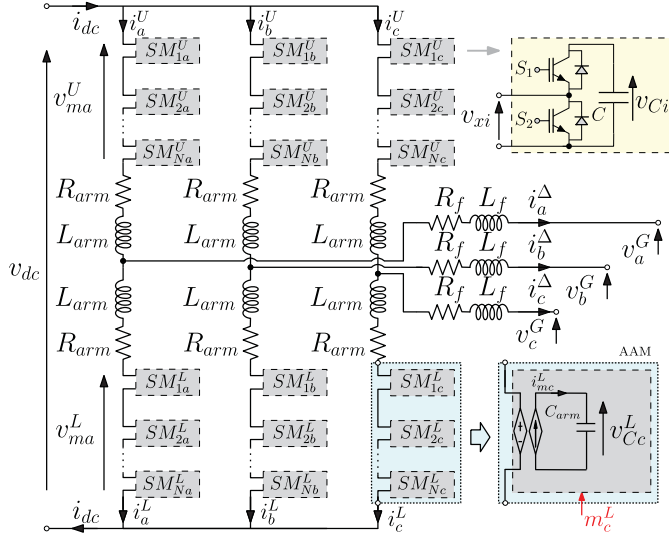
Fig. 2. MMC Topology and AAM (phase C).

Assuming that all the SM capacitor voltages are maintained in a close range, the series connection of SMs in each arm can be replaced by a circuit-based average model, corresponding to the well-known AAM, as indicated in Fig. 2 for the lower arm of phase c [4], [7]. If the MMC is modeled by the AAM representation, each arm appears as a controlled voltage source in the three-phase topology, while a power balance is established between the arm and its equivalent capacitance. Thus, each arm can be represented by a conventional power-balance-based average model of a single-phase VSC, with a modulated voltage source interfacing the filter inductor, and a controlled current source interfacing the capacitor-side.

The output of the controlled voltage and current sources of the AAM are here referred as the modulated voltages v_{mj}^U and v_{mj}^L and modulated currents i_{mj}^U and i_{mj}^L, for the upper (U) and lower (L) arms of a generic phase j, and are described by the following equations:

$$v_{mj}^U = m_j^U v_{Cj}^U, \quad v_{mj}^L = m_j^L v_{Cj}^L$$
$$i_{mj}^U = m_j^U i_j^U, \quad i_{mj}^L = m_j^L i_j^L \tag{1}$$

where v_{Cj}^U and v_{Cj}^L are, respectively, the voltages across the upper and lower arm equivalent capacitors. The corresponding modulation indices for the upper and lower arms are denoted as m_j^U and m_j^L, while i_j^U and i_j^L are the currents in the upper and lower arms, respectively.

B. Modeling of the MMC With $\Sigma-\Delta$ Variables in the Stationary abc Frame

As mentioned in the Introduction, the proposed state-space modeling approach adopts the $\Sigma-\Delta$ representation as opposed to the more commonly used *Upper–Lower* (U–L) arm notation, to ease the derivation of an MMC representation with SSTI solution. More precisely, under this $\Sigma-\Delta$ representation, it is possible to initially classify the 11 states and 6 control variables for an average model of a three-phase MMC into two frequency groups; i.e., the Δ variables that are associated with the fundamental frequency ω, and the Σ variables which are

in turn associated with -2ω. As will be further explained in Section II-C, the Δ variables can also contain a 3ω component and the Σ variables will contain a dc component. However, under balanced three-phase conditions, these components will be equal in all phases and can be represented separately as zero sequence components. It is therefore useful to redefine the voltages and currents that are defined in Fig. 2 using the $\Sigma-\Delta$ nomenclature, resulting in

$$i_j^\Delta \stackrel{\text{def}}{=} i_j^U - i_j^L, \quad i_j^\Sigma \stackrel{\text{def}}{=} (i_j^U + i_j^L)/2$$
$$v_{Cj}^\Delta \stackrel{\text{def}}{=} (v_{Cj}^U - v_{Cj}^L)/2, \quad v_{Cj}^\Sigma \stackrel{\text{def}}{=} (v_{Cj}^U + v_{Cj}^L)/2. \tag{2}$$

In this equation, i_j^Δ is the current flowing through the ac-side grid, whereas i_j^Σ is the well-known circulating current of the MMC. Moreover, v_{Cj}^Δ and v_{Cj}^Σ represent the difference and the sum of voltages across the upper and lower equivalent capacitors, respectively.

In addition, it is useful to define the modulation indices in the $\Sigma-\Delta$ representation as

$$m_j^\Delta \stackrel{\text{def}}{=} m_j^U - m_j^L, \quad m_j^\Sigma \stackrel{\text{def}}{=} m_j^U + m_j^L \tag{3}$$

and the modulated voltages from (1) as

$$v_{mj}^\Delta \stackrel{\text{def}}{=} \frac{-v_{mj}^U + v_{mj}^L}{2} = -\frac{m_j^\Delta v_{Cj}^\Sigma + m_j^\Sigma v_{Cj}^\Delta}{2}$$
$$v_{mj}^\Sigma \stackrel{\text{def}}{=} \frac{+v_{mj}^U + v_{mj}^L}{2} = +\frac{m_j^\Sigma v_{Cj}^\Sigma + m_j^\Delta v_{Cj}^\Delta}{2}. \tag{4}$$

1) AC-Grid Current Dynamics: The three-phase ac-grid currents dynamics $\boldsymbol{i_{abc}^\Delta}$ are expressed using vector nomenclature in the stationary frame as

$$L_{\text{eq}}^{\text{ac}} \frac{d\boldsymbol{i_{abc}^\Delta}}{dt} = \boldsymbol{v_{mabc}^\Delta} - \boldsymbol{v_{abc}^G} - R_{\text{eq}}^{\text{ac}}\boldsymbol{i_{abc}^\Delta} \tag{5}$$

where $\boldsymbol{v_{abc}^G}$ is the grid voltage vector defined as $[v_a^G \ v_b^G \ v_c^G]^\top$, whereas $\boldsymbol{v_{mabc}^\Delta}$ is the modulated voltage driving the ac-grid current defined as $[v_{ma}^\Delta \ v_{mb}^\Delta \ v_{mc}^\Delta]^\top$. These modulated voltages can be expressed as

$$\boldsymbol{v_{mabc}^\Delta} = -\frac{1}{2}(\boldsymbol{m_{abc}^\Delta} \circ \boldsymbol{v_{Cabc}^\Sigma} + \boldsymbol{m_{abc}^\Sigma} \circ \boldsymbol{v_{Cabc}^\Delta}) \tag{6}$$

where the *upper* and *lower* modulation indices and voltage variables were replaced by their $\Sigma-\Delta$ equivalents for convenience. It is worth noticing that the operator "$\circ$" will be used here to represent the element-wise multiplication of vectors (e.g., $\begin{bmatrix} a \\ b \end{bmatrix} \circ \begin{bmatrix} c \\ d \end{bmatrix} = \begin{bmatrix} ac \\ bd \end{bmatrix}$). Furthermore, $R_{\text{eq}}^{\text{ac}}$ and $L_{\text{eq}}^{\text{ac}}$ are the equivalent ac resistance and inductance, respectively, defined as $R_f + R_{arm}/2$ and $L_f + L_{arm}/2$.

2) Circulating Current Dynamics: The three-phase circulating currents dynamics in the stationary frame can be written using vector notation as

$$L_{arm} \frac{d\boldsymbol{i_{abc}^\Sigma}}{dt} = \frac{\boldsymbol{v_{dc}}}{2} - \boldsymbol{v_{mabc}^\Sigma} - R_{arm}\boldsymbol{i_{abc}^\Sigma} \tag{7}$$

where $\boldsymbol{v_{dc}}$ is defined as $[v_{dc} \ v_{dc} \ v_{dc}]^\top$ and $\boldsymbol{v_{mabc}^\Sigma}$ is the modulated voltage driving the circulating current defined as $[v_{ma}^\Sigma \ v_{mb}^\Sigma \ v_{mc}^\Sigma]^\top$. These voltage signals can be expressed as

$$\boldsymbol{v_{mabc}^\Sigma} = \frac{1}{2}(\boldsymbol{m_{abc}^\Sigma} \circ \boldsymbol{v_{Cabc}^\Sigma} + \boldsymbol{m_{abc}^\Delta} \circ \boldsymbol{v_{Cabc}^\Delta}) \tag{8}$$

where the *upper* and *lower* modulation indices and voltage variables were replaced by their $\Sigma-\Delta$ equivalents for convenience here as well.

3) Arm Capacitor Voltage Dynamics: Similarly, the dynamics of the voltage sum and difference between the equivalent capacitors of the AAM can be expressed, respectively, as

$$2C_{\text{arm}}\frac{dv_{Cabc}^{\Sigma}}{dt} = m_{abc}^{\Delta} \circ \frac{i_{abc}^{\Delta}}{2} + m_{abc}^{\Sigma} \circ i_{abc}^{\Sigma} \qquad (9)$$

$$2C_{\text{arm}}\frac{dv_{Cabc}^{\Delta}}{dt} = m_{abc}^{\Sigma} \circ \frac{i_{abc}^{\Delta}}{2} + m_{abc}^{\Delta} \circ i_{abc}^{\Sigma}. \qquad (10)$$

C. Simplified Frequency Analysis of the $\Sigma-\Delta$ Variables in Steady State

It is well known that under normal operating conditions the grid current i_{abc}^{Δ} of the MMC should contain only oscillations at the grid frequency ω. However, the circulating current usually consists of a dc value or a dc value in addition to oscillating signals at -2ω, depending on whether the second harmonic component is eliminated by control or not [3], [4]. Taking this into account in (5) and (7), it can be easily seen that the modulated voltages v_{mabc}^{Δ} should oscillate at ω, whereas v_{mabc}^{Σ} should have a dc component approximately equal to $v_{dc}/2$ and possibly a -2ω oscillation to shape the circulating current. A simplified assessment of the steady-state frequency components in the remaining state variables v_{Cabc}^{Σ} and v_{Cabc}^{Δ} can then be based on the following considerations.

In the definitions of the upper and lower modulated voltages given in (1), assume temporarily that the oscillatory components present in the aggregated arm capacitor voltages v_{Cj}^{U} and v_{Cj}^{L} are significantly smaller than their dc offset, which in turn is approximately equal to v_{dc} [4]. This assumption would imply that (6) and (8) could be simplified to $v_{mabc}^{\Delta} \approx m_{abc}^{\Delta} v_{dc}/2$ and $v_{mabc}^{\Sigma} \approx m_{abc}^{\Sigma} v_{dc}/2$. Moreover, since the steady-state frequency components of v_{mabc}^{Δ} and v_{mabc}^{Σ} are imposed by the desired shape of their corresponding associated currents as discussed above, m_{abc}^{Δ} should therefore oscillate at ω, whereas m_{abc}^{Σ} should consist of a dc component in addition to an optional -2ω frequency component in steady state. Taking this into account, it can be further assumed that $m_j^{\Delta} \approx \hat{m}\cos(\omega t)$ and $m_j^{\Sigma} \approx \hat{m}$, for a positive constant value $\hat{m} \leq 1$. By inspecting the right-hand side of (9), it can be seen that in steady state, the first product $m_j^{\Delta} i_j^{\Delta}/2$ gives a dc value in addition to an oscillatory signal at 2ω, while the second product $m_j^{\Sigma} i_j^{\Sigma}$ gives a dc value in case a constant value of i_{abc}^{Σ} is imposed by control (e.g., by the CCSC from [33]), or a dc value in addition to a 2ω component otherwise. Thus, both the cases will result in a dominant oscillation frequency of 2ω in v_{Cj}^{Σ}.

Similarly for v_{Cj}^{Δ}, the first product on the right-hand side of (10), $m_j^{\Sigma} i_j^{\Delta}/2$, oscillates at ω, while the second product $m_j^{\Delta} i_j^{\Sigma}$ oscillates at ω in the case the CCSC is used or will result in a signal oscillating at ω superimposed to one at 3ω otherwise. Note that if the assumption $m_j^{\Sigma} \approx 1$ is no longer considered, but instead m_{abc}^{Σ} is allowed to have a second harmonic component superimposed to its dc value, the first

$\omega, 3\omega$	$-2\omega, dc$
$i_j^{\Delta} = i_j^{U} - i_j^{L}$	$i_j^{\Sigma} = (i_j^{U} + i_j^{L})/2$
$v_{Cj}^{\Delta} = (-v_{Cj}^{U} + v_{Cj}^{L})/2$	$v_{Cj}^{\Sigma} = (v_{Cj}^{U} + v_{Cj}^{L})/2$
$v_{mj}^{\Delta} = (-v_{mj}^{U} + v_{mj}^{L})/2$	$v_{mj}^{\Sigma} = (v_{mj}^{U} + v_{mj}^{L})/2$
$m_j^{\Delta} = m_j^{U} - m_j^{L}$	$m_j^{\Sigma} = m_j^{U} + m_j^{L}$

term of (10) will also produce an additional component at 3ω.

As will be shown in the remainder of this paper, the third harmonic in the Δ variable will be captured and isolated by the zero sequence component after the application of Park's transformation at ω, without affecting its corresponding dq components. This is similar to the case for the Σ variables, as in addition to the -2ω signals, they present a dc value which will be isolated as a zero sequence component after the application of Park's transformation at -2ω, without affecting its dq components.

This initial classification of the state and control variables according to their main oscillation frequencies is summarized in Table I and is considered as the base for the methodology and derivations presented in the following section.

III. NONLINEAR TIME-INVARIANT MMC MODEL WITH VOLTAGE-BASED $\Sigma-\Delta$ REPRESENTATION IN dqz FRAME

In this section, the derivations needed for obtaining the time-invariant state-space representation of the MMC with voltage-based formulation are presented in detail on the basis of the approach in [31]. The formulation of the MMC variables such that the initial separation of frequency components can be achieved constitutes the basis for the proposed modeling approach, as illustrated in Fig. 3.

The illustration in Fig. 3 indicates that Park transformations at different frequencies will be used to derive dynamic equations for equivalent dqz variables that are SSTI and become dc-signals in their respective reference frames. More precisely, the Δ-variables (v_{Cabc}^{Δ}, i_{abc}^{Δ} and m_{abc}^{Δ}) are transformed into their dqz equivalents by means of a Park transformation P_{ω} at the grid fundamental frequency ω. By contrast, the Σ-variables (v_{Cabc}^{Σ}, i_{abc}^{Σ} and m_{abc}^{Σ}) are transformed into their dqz equivalents by means of a Park transformation $P_{-2\omega}$ at twice the grid frequency in negative sequence, -2ω. In addition, a transformation at 3ω will be applied to a virtual two-phase system established from the zero sequence of the voltage difference, v_{Cz}^{Δ}, for obtaining an SSTI representation of the third harmonic zero sequence component. The same approach will also be applied to the zero sequence of the modulation index difference m_z^{Δ}. The representation of the third harmonic zero sequence components as dq-variables in an SRRF at 3ω implies that the number of states and control variables for SSTI representation of a three-phase MMC will increase to 12 and 7, respectively, for representing the same dynamics as described by 11 states and 6 control
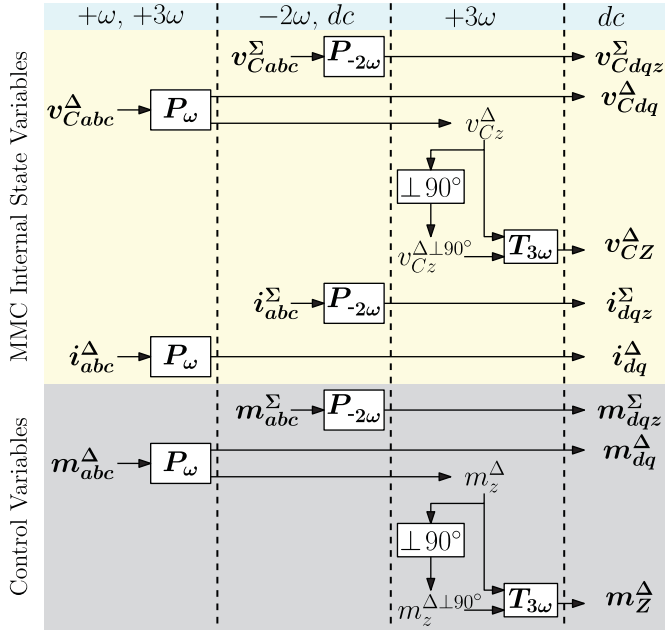
Fig. 3.   Proposed modeling approach based on three Park transformations for achieving an SSTI solution for all MMC variables.

variables in the conventional time-periodic per-phase AAM representation.

In the remainder of this section, the mathematical derivation of dynamic equations with SSTI solution representing the dynamics of a three-phase MMC will be expressed using the approach illustrated in Fig. 3. The mathematical reformulation consists in expressing the vector variables in the stationary abc frame as a function of their dqz equivalents at their respective rotating frequencies.

A. Voltage Difference Dynamics

1) Initial Formulation: The SSTI representation of the voltage difference dynamics is derived in the following. The starting point is indeed the SSTP dynamics given in (10), and recalled in (11a) for convenience. The first step consists in expressing the abc vectors in the stationary frame as functions of their respective dqz equivalents. This can be seen in (11b), where v_{Cabc}^{Δ}, m_{abc}^{Σ}, i_{abc}^{Δ}, m_{abc}^{Δ}, and i_{abc}^{Σ} have been, respectively, replaced by $P_{\omega}^{-1}v_{Cdqz}^{\Delta}$, $P_{-2\omega}^{-1}m_{dqz}^{\Sigma}$, $P_{\omega}^{-1}i_{dqz}^{\Delta}$, $P_{\omega}^{-1}m_{dqz}^{\Delta}$ and $P_{-2\omega}^{-1}i_{dqz}^{\Sigma}$. Notice that the choice of using the inverse Park transformation matrix at ω (P_{ω}^{-1}) or at -2ω ($P_{-2\omega}^{-1}$) is according to the frequency separation of the variables given in Table I and Fig. 3.

$$2C_{\text{arm}}\frac{dv_{Cabc}^{\Delta}}{dt} = m_{abc}^{\Sigma}\circ\frac{i_{abc}^{\Delta}}{2}+m_{abc}^{\Delta}\circ i_{abc}^{\Sigma} \qquad (11a)$$

$$\underbrace{2C_{\text{arm}}\frac{dP_{\omega}^{-1}}{dt}v_{Cdqz}^{\Delta} + 2C_{\text{arm}}P_{\omega}^{-1}\frac{dv_{Cdqz}^{\Delta}}{dt}}_{\Phi_A^{\Delta}}$$

$$= \underbrace{P_{-2\omega}^{-1}m_{dqz}^{\Sigma}\circ\frac{P_{\omega}^{-1}i_{dqz}^{\Delta}}{2}}_{\Phi_B^{\Delta}}+\underbrace{P_{\omega}^{-1}m_{dqz}^{\Delta}\circ P_{-2\omega}^{-1}i_{dqz}^{\Sigma}}_{\Phi_C^{\Delta}}$$

$$\qquad\qquad (11b)$$

The equation expressed in (11b) must be multiplied by the Park transformation matrix at the angular frequency ω, so that it can be solved for dv_{Cdqz}^{Δ}/dt.

Multiplying Φ_A^{Δ} by P_{ω}, gives

$$P_{\omega}\Phi_A^{\Delta} = 2C_{\text{arm}}J_{\omega}v_{Cdqz}^{\Delta} + 2C_{\text{arm}}\frac{dv_{Cdqz}^{\Delta}}{dt} \qquad (12)$$

where J_{ω} is defined as

$$J_{\omega} \overset{\text{def}}{=} \begin{bmatrix} 0 & \omega & 0 \\ -\omega & 0 & 0 \\ 0 & 0 & 0 \end{bmatrix}. \qquad (13)$$

Furthermore, multiplying Φ_B^{Δ} by P_{ω} gives

$$P_{\omega}\Phi_B^{\Delta} = P_{\omega}\left(P_{-2\omega}^{-1}m_{dqz}^{\Sigma}\circ\frac{P_{\omega}^{-1}i_{dqz}^{\Delta}}{2}\right) = M_{\Phi_B}^{\Delta}\begin{bmatrix} i_d^{\Delta} \\ i_q^{\Delta} \\ i_z^{\Delta} \end{bmatrix} \qquad (14)$$

where $M_{\Phi_B}^{\Delta}$ is expressed in (15), as shown at the bottom of this page. For simplicity, it will be considered that the system under study is a three-phase three-wire system that does not allow the existence of the zero sequence grid current, i.e., $i_z^{\Delta} = 0$. Thus, the terms associated with i_z^{Δ} in (14) are printed in gray. Under this assumption, the dq components of (14) are time-invariant, as the 3ω oscillatory signals that appear in $M_{\Phi_B}^{\Delta}$ are either multiplied by i_z^{Δ} (third column of the matrix) or associated with the zero sequence component (third row of the matrix). However, it is possible to rewrite also the dynamics of v_{Cz}^{Δ} in SSTI form by means of additional mathematical manipulations, as will be demonstrated separately.

Finally, multiplying Φ_C^{Δ} by P_{ω} gives

$$P_{\omega}\Phi_C^{\Delta} = P_{\omega}\left(P_{\omega}^{-1}m_{dqz}^{\Delta}\circ P_{-2\omega}^{-1}i_{dqz}^{\Sigma}\right) = M_{\Phi_C}^{\Delta}\begin{bmatrix} i_d^{\Sigma} \\ i_q^{\Sigma} \\ i_z^{\Sigma} \end{bmatrix} \qquad (16)$$

where $M_{\Phi_C}^{\Delta}$ is expressed in (17), as shown at the bottom of the next page. Here, $M_{\Phi_C}^{\Delta}$ requires further mathematical manipulation to achieve the desired SSTI performance, as the 3ω signals also appear. Moreover, they affect not only the zero sequence as in the previous case, but the dq components as well.

Replacing the definitions given in (12), (14), and (16) in $P_{\omega}^{-1}\Phi_A^{\Delta} = P_{\omega}^{-1}\Phi_B^{\Delta} + P_{\omega}^{-1}\Phi_C^{\Delta}$ and solving for the voltage

$$M_{\Phi_B}^{\Delta} = \frac{1}{4}\begin{bmatrix} m_d^{\Sigma}+2m_z^{\Sigma} & -m_q^{\Sigma} & 2m_d^{\Sigma}\cos(3\omega t)-2m_q^{\Sigma}\sin(3\omega t) \\ -m_q^{\Sigma} & -m_d^{\Sigma}+2m_z^{\Sigma} & 2m_q^{\Sigma}\cos(3\omega t)+2m_d^{\Sigma}\sin(3\omega t) \\ \hline m_d^{\Sigma}\cos(3\omega t)-m_q^{\Sigma}\sin(3\omega t) & m_q^{\Sigma}\cos(3\omega t)+m_d^{\Sigma}\sin(3\omega t) & 2m_z^{\Sigma} \end{bmatrix} \qquad (15)$$

difference dynamics in their dqz coordinates results in

$$\frac{dv_{Cdqz}^\Delta}{dt} = \frac{1}{2C_{arm}}\left(M_{\Phi_B}^\Delta\begin{bmatrix}i_d^\Delta\\i_q^\Delta\\i_z^\Delta\end{bmatrix} + M_{\Phi_C}^\Delta\begin{bmatrix}i_d^\Sigma\\i_q^\Sigma\\i_z^\Sigma\end{bmatrix}\right) - J_\omega v_{Cdqz}^\Delta.$$

(18)

Since neither $M_{\Phi_B}^\Delta$ nor $M_{\Phi_C}^\Delta$ is SSTI, the expression in (18) does not directly provide an SSTI solution. This issue is treated in the following.

2) Deriving the SSTI dq Dynamics of (18): First, the dq dynamics of (18) are addressed. Since it is assumed that $i_z^\Delta = 0$, only $M_{\Phi_C}^\Delta$ hinders an SSTI representation of the dq dynamics, due to the appearance of the $\cos(3\omega t)$ and $\sin(3\omega t)$ in the 2×2 submatrix at the upper left corner of $M_{\Phi_C}^\Delta$ in (17), referred to as $M_{\Phi_C}^{\Delta 2\times2}$. A possible simplification results from assuming that the MMC control will always set m_z^Δ to zero, as was done in [31], since m_z^Δ multiplies all of the 3ω oscillating signals. However, this leads to a restrictive model from a control perspective, and therefore this assumption is avoided here.

Taking inspiration from common engineering practices to increase controllability in three-phase VSCs [37], the proposed solution is to redefine m_z^Δ as a third harmonic injection given by

$$m_z^\Delta \overset{def}{=} m_{Z_d}^\Delta\cos(3\omega t) + m_{Z_q}^\Delta\sin(3\omega t)$$

(19)

where $m_{Z_d}^\Delta$ and $m_{Z_q}^\Delta$ are two SSTI variables that will define the amplitude and phase angle of the third harmonic oscillations in m_z^Δ.

Replacing the new definition from (19) in (17), results in the submatrix

$$M_{\Phi_C}^{\Delta 2\times2} = \frac{1}{2}\begin{bmatrix}(m_d^\Delta+m_{Z_d}^\Delta) & -(m_q^\Delta+m_{Z_q}^\Delta)\\-(m_q^\Delta-m_{Z_q}^\Delta) & -(m_d^\Delta-m_{Z_d}^\Delta)\end{bmatrix}$$
$$+\underbrace{\begin{bmatrix}\cos(6\omega t) & \sin(6\omega t)\\\sin(6\omega t) & -\cos(6\omega t)\end{bmatrix}\begin{bmatrix}m_{Z_d}^\Delta & m_{Z_q}^\Delta\\m_{Z_q}^\Delta & -m_{Z_d}^\Delta\end{bmatrix}}_{\approx0}.$$

(20)

Thus, the elements with 3ω oscillations are replaced by a dc-component and an oscillation at 6ω. As will be confirmed via time-domain simulations, the 6ω oscillations are small and can be neglected when studying the dynamics of the MMC.

3) Deriving SSTI Expressions for the Zero Sequence Dynamics of (18): For convenience, the zero sequence state

equation from (18) is rewritten explicitly as

$$C_{arm}\frac{dv_{Cz}^\Delta}{dt} = \frac{m_z^\Delta}{2}i_z^\Sigma$$
$$+\frac{1}{8}(m_d^\Sigma i_d^\Delta + m_q^\Sigma i_q^\Delta + 2m_d^\Delta i_d^\Sigma + 2m_q^\Delta i_q^\Sigma)\cos(3\omega t)$$
$$+\frac{1}{8}(-m_q^\Sigma i_d^\Delta + m_d^\Sigma i_q^\Delta + 2m_q^\Delta i_d^\Sigma - 2m_d^\Delta i_q^\Sigma)\sin(3\omega t).$$

(21)

By writing this equation on the same form as defined by (19), the zero sequence dynamics of v_{Cz}^Δ can be expressed as

$$\frac{dv_{Cz}^\Delta}{dt} = \frac{1}{C_{arm}}[\Psi_d\cos(3\omega t) + \Psi_q\sin(3\omega t)]$$

(22)

where Ψ_d and Ψ_q are defined as:

$$\Psi_d = \frac{1}{8}(m_d^\Sigma i_d^\Delta + m_q^\Sigma i_q^\Delta + 2m_d^\Delta i_d^\Sigma + 2m_q^\Delta i_q^\Sigma + 4m_{Z_d}^\Delta i_z^\Sigma)$$

$$\Psi_q = \frac{1}{8}(-m_q^\Sigma i_d^\Delta + m_d^\Sigma i_q^\Delta + 2m_q^\Delta i_d^\Sigma - 2m_d^\Delta i_q^\Sigma + 4m_{Z_q}^\Delta i_z^\Sigma).$$

Since the zero sequence dynamics in (22) are still time-varying in steady state, further reformulation is necessary to obtain the desired model with SSTI solution. This can be obtained by defining an auxiliary virtual state $v_{CZ_\beta}^\Delta$, shifted $90°$ with respect to the original "single-phase" time-periodic voltage difference signal v_{Cz}^Δ according to the approach from [31]. This approach is conceptually similar to the commonly applied strategy of generating a virtual two-phase system for representing single-phase systems in an SRRF [41]. However, since the amplitudes of the different sine and cosine components, Ψ_d and Ψ_q, are defined by SSTI variables, the virtual signal $v_{CZ_\beta}^\Delta$ can be identified directly from the existing variables without any additional delay.

The real and virtual voltage difference zero sequence variables can be labeled as $v_{CZ_\alpha}^\Delta$ and $v_{CZ_\beta}^\Delta$, and together they define an orthogonal $\alpha\beta$-system. This $\alpha\beta$-system can be expressed by

$$\frac{dv_{CZ_\alpha}^\Delta}{dt} = \frac{1}{C_{arm}}[\Psi_d\cos(3\omega t) + \Psi_q\sin(3\omega t)]$$ (23a)
$$\frac{dv_{CZ_\beta}^\Delta}{dt} = \frac{1}{C_{arm}}[\Psi_d\sin(3\omega t) - \Psi_q\cos(3\omega t)]$$ (23b)

where (23a) is identical to (22), while (23b) is obtained by replacing the terms $\cos(3\omega t)$ and $\sin(3\omega t)$ that appear in (22) by $\sin(3\omega t)$ and $-\cos(3\omega t)$, respectively.

Defining $v_{CZ_{\alpha\beta}}^\Delta \overset{def}{=} [v_{CZ_\alpha}^\Delta\ v_{CZ_\beta}^\Delta]^\top$, (23a) and (23b) can be written in compact form as

$$\frac{dv_{CZ_{\alpha\beta}}^\Delta}{dt} = \frac{1}{C_{arm}}\{T_{3\omega}^{-1}[\Psi_d\ \Psi_q]^\top\}$$

(24)

$$M_{\Phi_C}^\Delta = \frac{1}{2}\left[\begin{array}{cc:c}m_d^\Delta+2m_z^\Delta\cos(3\omega t) & -m_q^\Delta-2m_z^\Delta\sin(3\omega t) & 2m_d^\Delta\\-m_q^\Delta+2m_z^\Delta\sin(3\omega t) & -m_d^\Delta+2m_z^\Delta\cos(3\omega t) & 2m_q^\Delta\\\hdashline m_d^\Delta\cos(3\omega t)+m_q^\Delta\sin(3\omega t) & m_q^\Delta\cos(3\omega t)-m_d^\Delta\sin(3\omega t) & 2m_z^\Delta\end{array}\right]$$

(17)

where $T_{3\omega}$ is a rotational transformation at 3ω as defined by

$$T_{3\omega} \overset{\text{def}}{=} \begin{bmatrix} \cos(3\omega t) & \sin(3\omega t) \\ \sin(3\omega t) & -\cos(3\omega t) \end{bmatrix}. \tag{25}$$

Furthermore, by defining $v_{CZ}^{\Delta} \overset{\text{def}}{=} [v_{CZ_d}^{\Delta} v_{CZ_q}^{\Delta}]^{\top}$ such that

$$v_{CZ}^{\Delta} = T_{3\omega} v_{CZ_{\alpha\beta}}^{\Delta}, \tag{26}$$

replacing (26) into (24), multiplying by $T_{3\omega}$, and solving for the dynamics of v_{CZ}^{Δ} gives

$$\frac{dv_{CZ}^{\Delta}}{dt} = \frac{1}{C_{\text{arm}}} \left\{ [\Psi_d \ \ \Psi_q]^{\top} - C_{\text{arm}} J_{3\omega} v_{CZ}^{\Delta} \right\} \tag{27}$$

where $J_{3\omega}$ is defined as

$$J_{3\omega} \overset{\text{def}}{=} \begin{bmatrix} 0 & -3\omega \\ 3\omega & 0 \end{bmatrix}. \tag{28}$$

Equation (27) will then produce an SSTI representation for the dynamics of the zero sequence voltage difference v_{Cz}^{Δ}. The original oscillating SSTP signal of v_{Cz}^{Δ} can always be recreated by solving for $v_{CZ_{\alpha}}^{\Delta} = v_{Cz}^{\Delta}$ in (26), resulting in

$$v_{Cz}^{\Delta} = v_{CZ_d}^{\Delta} \cos(3\omega t) + v_{CZ_q}^{\Delta} \sin(3\omega t). \tag{29}$$

4) Final Formulation: To summarize the SSTI voltage difference equations, it is useful to redefine a new augmented voltage vector v_{CdqZ}^{Δ} (with capital Z), as

$$v_{CdqZ}^{\Delta} \overset{\text{def}}{=} \begin{bmatrix} v_{Cd}^{\Delta} & v_{Cq}^{\Delta} & v_{CZ_d}^{\Delta} & v_{CZ_q}^{\Delta} \end{bmatrix}^{\top} \tag{30}$$

as well as for the "Δ" modulation indices, as

$$m_{dqZ}^{\Delta} \overset{\text{def}}{=} \begin{bmatrix} m_d^{\Delta} & m_q^{\Delta} & m_{Z_d}^{\Delta} & m_{Z_q}^{\Delta} \end{bmatrix}^{\top}. \tag{31}$$

Considering the new definitions $v_{CZ_d}^{\Delta}$, $v_{CZ_q}^{\Delta}$, and their associated dynamics given by (27), and taking into account the modified (sub)matrix $M_{\Phi_C}^{\Delta 2 \times 2}$ given in (20), the SSTP dynamics of v_{Cdqz}^{Δ} from (18) may be now expressed by equivalent state equations with SSTI characteristics, by means of the 4×1 state vector v_{CdqZ}^{Δ} as shown in (32), with J_G defined in (33)

$$C_{\text{arm}} \frac{dv_{CdqZ}^{\Delta}}{dt} = -J_G C_{\text{arm}} v_{CdqZ}^{\Delta}$$

$$+ \frac{1}{8} \begin{bmatrix} (m_d^{\Sigma} + 2m_z^{\Sigma}) & -m_q^{\Sigma} \\ -m_q^{\Sigma} & (-m_d^{\Sigma} + 2m_z^{\Sigma}) \\ m_d^{\Sigma} & m_q^{\Sigma} \\ -m_q^{\Sigma} & m_d^{\Sigma} \end{bmatrix} i_{dq}^{\Delta}$$

$$+ \frac{1}{4} \begin{bmatrix} (m_d^{\Delta} + m_{Z_d}^{\Delta}) & -(m_q^{\Delta} + m_{Z_q}^{\Delta}) & m_d^{\Delta} \\ -(m_q^{\Delta} - m_{Z_q}^{\Delta}) & -(m_d^{\Delta} - m_{Z_d}^{\Delta}) & m_q^{\Delta} \\ m_d^{\Delta} & m_q^{\Delta} & 2m_{Z_d}^{\Delta} \\ m_q^{\Delta} & -m_d^{\Delta} & 2m_{Z_q}^{\Delta} \end{bmatrix} i_{dqz}^{\Sigma}. \tag{32}$$

$$J_G \overset{\text{def}}{=} \begin{bmatrix} 0 & \omega & \mathbf{0}_{2 \times 2} \\ -\omega & 0 & \\ \mathbf{0}_{2 \times 2} & J_{3\omega} \end{bmatrix}. \tag{33}$$

B. Voltage Sum Dynamics

1) Initial Formulation: The SSTI dynamics of the voltage sum can be derived in a similar way as for the voltage difference. The starting point is indeed the SSTP dynamics given by (9), as recalled in (34a) for convenience. The first step consists in expressing the stationary frame abc vectors present in (34a), as functions of their respective dqz equivalents. This is done in (34b), where v_{Cabc}^{Σ}, m_{abc}^{Δ}, i_{abc}^{Δ}, m_{abc}^{Σ} and i_{abc}^{Σ} have been, respectively, replaced by $P_{-2\omega}^{-1} v_{Cdqz}^{\Sigma}$, $P_{\omega}^{-1} m_{dqz}^{\Delta}$, $P_{\omega}^{-1} i_{dqz}^{\Delta}$, $P_{-2\omega}^{-1} m_{dqz}^{\Sigma}$ and $P_{-2\omega}^{-1} i_{dqz}^{\Sigma}$. Notice that the choice of using the inverse Park transformation at ω (P_{ω}^{-1}) or at -2ω ($P_{-2\omega}^{-1}$) is again according to the frequency separation of the variables given in Table I and Fig. 3.

The resulting equation can be divided into three parts: Φ_A^{Σ}, Φ_B^{Σ}, and Φ_C^{Σ}, as indicated in (34b). These three parts are treated consecutively in the following:

$$2C_{\text{arm}} \frac{dv_{Cabc}^{\Sigma}}{dt} = m_{abc}^{\Delta} \circ \frac{i_{abc}^{\Delta}}{2} + m_{abc}^{\Sigma} \circ i_{abc}^{\Sigma} \tag{34a}$$

$$\underbrace{2C_{\text{arm}} \frac{dP_{-2\omega}^{-1}}{dt} v_{Cdqz}^{\Sigma} + 2C_{\text{arm}} P_{-2\omega}^{-1} \frac{dv_{Cdqz}^{\Sigma}}{dt}}_{\Phi_A^{\Sigma}}$$

$$= \underbrace{P_{\omega}^{-1} m_{dqz}^{\Delta} \circ \frac{P_{\omega}^{-1} i_{dqz}^{\Delta}}{2}}_{\Phi_B^{\Sigma}} + \underbrace{P_{-2\omega}^{-1} m_{dqz}^{\Sigma} \circ P_{-2\omega}^{-1} i_{dqz}^{\Sigma}}_{\Phi_C^{\Sigma}}. \tag{34b}$$

The equation expressed in (34b), needs to be multiplied by Park's transformation at -2ω, so that it can be solved for dv_{Cdqz}^{Σ}/dt. Multiplying Φ_A^{Σ} by $P_{-2\omega}$ gives

$$P_{-2\omega} \Phi_A^{\Sigma} = 2C_{\text{arm}} J_{-2\omega} v_{Cdqz}^{\Sigma} + 2C_{\text{arm}} \frac{dv_{Cdqz}^{\Sigma}}{dt} \tag{35}$$

where $J_{-2\omega}$ is defined as $-2J_{\omega}$. Furthermore, multiplying Φ_B^{Σ} by $P_{-2\omega}$ gives (36), where $M_{\Phi_B}^{\Sigma}$ is expressed in (37), as shown at the bottom of the next page.

$$P_{-2\omega} \Phi_B^{\Sigma} = P_{-2\omega} \left(P_{\omega}^{-1} m_{dqz}^{\Delta} \circ P_{\omega}^{-1} \frac{i_{dqz}^{\Delta}}{2} \right) = M_{\Phi_B}^{\Sigma} \begin{bmatrix} i_d^{\Delta} \\ i_q^{\Delta} \\ i_z^{\Delta} \end{bmatrix}. \tag{36}$$

As mentioned, it is assumed that there cannot be any zero sequence grid current, i.e., $i_z^{\Delta} = 0$ (as indicated by the gray color). However, (36) still does not produce an SSTI solution, as the elements in the upper left 2×2 submatrix of $M_{\Phi_B}^{\Sigma}$ in (37) contain sine and cosine signals oscillating at 3ω. Note that this is also the case for the terms printed in gray in (37), but they can be disregarded since they are multiplied by $i_z^{\Delta} = 0$.

To address the remaining 3ω terms in (37), the same solution as used in the previous section is applied. Since all the oscillating terms are multiplied by m_z^{Δ}, it is convenient to redefine m_z^{Δ} by a third harmonic injection according to (19), as a function of the SSTI virtual variables $m_{Z_d}^{\Delta}$ and

$m_{Z_q}^{\Delta}$. Replacing (19) into (37) allows rewriting (36) as (38), as shown at the bottom of this page. This equation will become time invariant if it can be assumed that the oscillatory signals at 6ω are negligible, which can be confirmed by time-domain simulations.

In a similar fashion, the second component on the right-hand side of (34b), $\boldsymbol{\Phi}_C^{\Sigma}$, is multiplied by $\boldsymbol{P}_{-2\omega}$, resulting in (39), as shown at the bottom of this page, which can be considered SSTI if the sixth harmonic components are neglected. Here again, the validity of this approximation can be confirmed via time-domain simulations.

2) Final Formulation: The SSTI dynamics of the voltage sum vector $\boldsymbol{v}_{Cdqz}^{\Sigma}$ are found by introducing (35) and the SSTI parts of (38) and (39) into (34b) and solving for $d\boldsymbol{v}_{Cdqz}^{\Sigma}/dt$, resulting in

$$
C_{\mathrm{arm}}\frac{d\boldsymbol{v}_{Cdqz}^{\Sigma}}{dt} = -\boldsymbol{J}_{-2\omega}C_{\mathrm{arm}}\boldsymbol{v}_{Cdqz}^{\Sigma}
$$
$$
+\frac{1}{4}\begin{bmatrix} 2m_z^{\Sigma} & 0 & 2m_d^{\Sigma} \\ 0 & 2m_z^{\Sigma} & 2m_q^{\Sigma} \\ m_d^{\Sigma} & m_q^{\Sigma} & 2m_z^{\Sigma} \end{bmatrix}\boldsymbol{i}_{dqz}^{\Sigma}
$$
$$
+\frac{1}{8}\begin{bmatrix} (m_d^{\Delta}+m_{Z_d}^{\Delta}) & -(m_q^{\Delta}-m_{Z_q}^{\Delta}) \\ -(m_q^{\Delta}+m_{Z_q}^{\Delta}) & -(m_d^{\Delta}-m_{Z_d}^{\Delta}) \\ m_d^{\Delta} & m_q^{\Delta} \end{bmatrix}\boldsymbol{i}_{dq}^{\Delta}. \quad (40)
$$

C. Circulating Current Dynamics

The SSTI dynamics for the circulating current are derived in the following. First, the equation of the stationary frame dynamics from (7), as recalled in (41a) is rewritten by expressing the *abc* vectors in the equation as a function of their *dqz* equivalents, as indicated in (41b)

$$
L_{\mathrm{arm}}\frac{d\boldsymbol{i}_{abc}^{\Sigma}}{dt} = \frac{v_{dc}}{2} - \boldsymbol{v}_{mabc}^{\Sigma} - R_{\mathrm{arm}}\boldsymbol{i}_{abc}^{\Sigma} \quad (41a)
$$

$$
L_{\mathrm{arm}}\frac{d\boldsymbol{P}_{-2\omega}^{-1}}{dt}\boldsymbol{i}_{dqz}^{\Sigma} + L_{\mathrm{arm}}\boldsymbol{P}_{-2\omega}^{-1}\frac{d\boldsymbol{i}_{dqz}^{\Sigma}}{dt}
$$
$$
= \frac{v_{dc}}{2} - \boldsymbol{P}_{-2\omega}^{-1}\boldsymbol{v}_{mdqz}^{\Sigma} - R_{\mathrm{arm}}\boldsymbol{P}_{-2\omega}^{-1}\boldsymbol{i}_{dqz}^{\Sigma}. \quad (41b)
$$

Multiplying (41b) by $\boldsymbol{P}_{-2\omega}$ and solving for $d\boldsymbol{i}_{dqz}^{\Sigma}/dt$ gives

$$
L_{\mathrm{arm}}\frac{d\boldsymbol{i}_{dqz}^{\Sigma}}{dt} = \begin{bmatrix} 0 \\ 0 \\ \dfrac{v_{dc}}{2} \end{bmatrix} - \boldsymbol{v}_{mdqz}^{\Sigma} - (R_{\mathrm{arm}} + L_{\mathrm{arm}}\boldsymbol{J}_{-2\omega})\boldsymbol{i}_{dqz}^{\Sigma}
$$
$$
(42)
$$

where $\boldsymbol{v}_{mdqz}^{\Sigma} \overset{\mathrm{def}}{=} \boldsymbol{P}_{-2\omega}^{-1}\boldsymbol{v}_{mabc}^{\Sigma}$, and $\boldsymbol{v}_{mabc}^{\Sigma}$ is defined in (8). Nonetheless, in order to assess if (42) is SSTI, $\boldsymbol{v}_{mdqz}^{\Sigma}$ needs to be rewritten by expressing the *abc* vectors in the equation as a function of their *dqz* equivalents, resulting in

$$
\boldsymbol{v}_{mdqz}^{\Sigma} = \frac{1}{2}\boldsymbol{P}_{-2\omega}\big(\boldsymbol{P}_{-2\omega}^{-1}\boldsymbol{m}_{dqz}^{\Sigma} \circ \boldsymbol{P}_{-2\omega}^{-1}\boldsymbol{v}_{Cdqz}^{\Sigma}
$$
$$
+ \boldsymbol{P}_{\omega}^{-1}\boldsymbol{m}_{dqz}^{\Delta} \circ \boldsymbol{P}_{\omega}^{-1}\boldsymbol{v}_{Cdqz}^{\Delta}\big) \quad (43a)
$$

$$
\boldsymbol{v}_{mdqz}^{\Sigma} = \boldsymbol{M}_{\boldsymbol{\Psi}_B}^{\Sigma}\begin{bmatrix} v_{Cd}^{\Sigma} \\ v_{Cq}^{\Sigma} \\ v_{Cz}^{\Sigma} \end{bmatrix} + \boldsymbol{M}_{\boldsymbol{\Psi}_C}^{\Sigma}\begin{bmatrix} v_{Cd}^{\Delta} \\ v_{Cq}^{\Delta} \\ v_{Cz}^{\Delta} \end{bmatrix}, \quad (43b)
$$

where $\boldsymbol{M}_{\boldsymbol{\Psi}_B}^{\Sigma}$ and $\boldsymbol{M}_{\boldsymbol{\Psi}_C}^{\Sigma}$ are expressed in (44) and (45), respectively, as shown at the top of the next page.

If the sixth harmonic components are negligible, as can be confirmed by time-domain simulations, $\boldsymbol{M}_{\boldsymbol{\Psi}_B}^{\Sigma}$ given in (44) can be considered as SSTI. However, this is not the case for $\boldsymbol{M}_{\boldsymbol{\Psi}_C}^{\Sigma}$ given in (45), as it presents nonnegligible third harmonic oscillations. To overcome this obstacle, it is necessary to replace into (45) and (43) the definitions of m_z^{Δ} and v_{Cz}^{Δ} given in (19) and (29), respectively. This results in the following definition

$$
\boldsymbol{v}_{mdqz}^{\Sigma} = \boldsymbol{M}_{\boldsymbol{\Psi}_B}^{\Sigma}\begin{bmatrix} v_{Cd}^{\Sigma} \\ v_{Cq}^{\Sigma} \\ v_{Cz}^{\Sigma} \end{bmatrix} + \boldsymbol{M}_{\boldsymbol{\Psi}_C}^{\Sigma\star}\begin{bmatrix} v_{Cd}^{\Delta} \\ v_{Cq}^{\Delta} \\ v_{CZ_d}^{\Delta} \\ v_{CZ_q}^{\Delta} \end{bmatrix}, \quad (46)
$$

where $\boldsymbol{M}_{\boldsymbol{\Psi}_C}^{\Sigma\star}$ is given by

$$
\boldsymbol{M}_{\boldsymbol{\Psi}_C}^{\Sigma\star} = \frac{1}{4}\begin{bmatrix} m_d^{\Delta}+m_{Z_d}^{\Delta} & -m_q^{\Delta}+m_{Z_q}^{\Delta} & m_d^{\Delta} & m_q^{\Delta} \\ -m_q^{\Delta}-m_{Z_q}^{\Delta} & -m_d^{\Delta}+m_{Z_d}^{\Delta} & m_q^{\Delta} & -m_d^{\Delta} \\ m_d^{\Delta} & m_q^{\Delta} & m_{Z_d}^{\Delta} & m_{Z_q}^{\Delta} \end{bmatrix}
$$
$$
+ \mathcal{H}_{6\omega t}. \quad (47)
$$

$$
\boldsymbol{M}_{\boldsymbol{\Phi}_B}^{\Sigma} = \frac{1}{4}\begin{bmatrix} m_d^{\Delta}+2m_z^{\Delta}\cos(3\omega t) & -m_q^{\Delta}+2m_z^{\Delta}\sin(3\omega t) & 2\left(m_d^{\Delta}\cos(3\omega t)+m_q^{\Delta}\sin(3\omega t)\right) \\ -m_q^{\Delta}-2m_z^{\Delta}\sin(3\omega t) & -m_d^{\Delta}+2m_z^{\Delta}\cos(3\omega t) & 2\left(m_q^{\Delta}\cos(3\omega t)-m_d^{\Delta}\sin(3\omega t)\right) \\ \hline m_d^{\Delta} & m_q^{\Delta} & 2m_z^{\Delta} \end{bmatrix} \quad (37)
$$

$$
\boldsymbol{P}_{-2\omega}\boldsymbol{\Phi}_B^{\Sigma} = \frac{1}{4}\begin{bmatrix} (m_d^{\Delta}+m_{Z_d}^{\Delta})i_d^{\Delta} - (m_q^{\Delta}-m_{Z_q}^{\Delta})i_q^{\Delta} \\ -(m_q^{\Delta}+m_{Z_q}^{\Delta})i_d^{\Delta} - (m_d^{\Delta}-m_{Z_d}^{\Delta})i_q^{\Delta} \\ m_d^{\Delta}i_d^{\Delta}+m_q^{\Delta}i_q^{\Delta} \end{bmatrix} + \underbrace{\frac{1}{4}\begin{bmatrix} \cos(6\omega t) & -\sin(6\omega t) & 0 \\ -\sin(6\omega t) & -\cos(6\omega t) & 0 \\ 0 & 0 & 0 \end{bmatrix}\begin{bmatrix} m_{Z_d}^{\Delta}i_d^{\Delta}-m_{Z_q}^{\Delta}i_q^{\Delta} \\ -m_{Z_q}^{\Delta}i_d^{\Delta}-m_{Z_d}^{\Delta}i_q^{\Delta} \\ 0 \end{bmatrix}}_{\approx 0} \quad (38)
$$

$$
\boldsymbol{P}_{-2\omega}\boldsymbol{\Phi}_C^{\Sigma} = \frac{1}{2}\begin{bmatrix} 2m_z^{\Sigma}i_d^{\Sigma}+2m_d^{\Sigma}i_z^{\Sigma} \\ 2m_z^{\Sigma}i_q^{\Sigma}+2m_q^{\Sigma}i_z^{\Sigma} \\ m_d^{\Sigma}i_d^{\Sigma}+m_q^{\Sigma}i_q^{\Sigma}+2m_z^{\Sigma}i_z^{\Sigma} \end{bmatrix} + \underbrace{\frac{1}{2}\begin{bmatrix} \left(m_d^{\Sigma}i_d^{\Sigma}-m_q^{\Sigma}i_q^{\Sigma}\right)\cos(6\omega t) - \left(m_q^{\Sigma}i_d^{\Sigma}+m_d^{\Sigma}i_q^{\Sigma}\right)\sin(6\omega t) \\ \left(-m_q^{\Sigma}i_d^{\Sigma}+m_d^{\Sigma}i_q^{\Sigma}\right)\sin(6\omega t) - \left(m_q^{\Sigma}i_d^{\Sigma}+m_d^{\Sigma}i_q^{\Sigma}\right)\cos(6\omega t) \\ 0 \end{bmatrix}}_{\approx 0} \quad (39)
$$

$$
M_{\Psi_B}^{\Sigma} = \frac{1}{4}\begin{bmatrix} 2m_z^{\Sigma} & 0 & 2m_d^{\Sigma} \\ 0 & 2m_z^{\Sigma} & 2m_q^{\Sigma} \\ m_d^{\Sigma} & m_q^{\Sigma} & 2m_z^{\Sigma} \end{bmatrix} + \underbrace{\begin{bmatrix} m_d^{\Sigma}\cos(6\omega t) - m_q^{\Sigma}\sin(6\omega t) & -m_q^{\Sigma}\cos(6\omega t) - m_d^{\Sigma}\sin(6\omega t) & 0 \\ -m_q^{\Sigma}\cos(6\omega t) - m_d^{\Sigma}\sin(6\omega t) & -m_d^{\Sigma}\cos(6\omega t) + m_q^{\Sigma}\sin(6\omega t) & 0 \\ 0 & 0 & 0 \end{bmatrix}}_{\approx 0} \tag{44}
$$

$$
M_{\Psi_C}^{\Sigma} = \frac{1}{4}\begin{bmatrix} m_d^{\Delta} + 2m_z^{\Delta}\cos(3\omega t) & -m_q^{\Delta} + 2m_z^{\Delta}\sin(3\omega t) & 2m_d^{\Delta}\cos(3\omega t) + 2m_q^{\Delta}\sin(3\omega t) \\ -m_q^{\Delta} - 2m_z^{\Delta}\sin(3\omega t) & -m_d^{\Delta} + 2m_z^{\Delta}\cos(3\omega t) & -2m_d^{\Delta}\sin(3\omega t) + 2m_q^{\Delta}\cos(3\omega t) \\ m_d^{\Delta} & m_q^{\Delta} & 2m_z^{\Delta} \end{bmatrix} \tag{45}
$$

$$
\mathcal{H}_{6\omega t} = \begin{bmatrix} m_{Z_d}^{\Delta}\cos(6\omega t) + m_{Z_q}^{\Delta}\sin(6\omega t) & m_{Z_d}^{\Delta}\sin(6\omega t) - m_{Z_q}^{\Delta}\cos(6\omega t) & m_d^{\Delta}\cos(6\omega t) + m_q^{\Delta}\sin(6\omega t) & -m_q^{\Delta}\cos(6\omega t) + m_d^{\Delta}\sin(6\omega t) \\ -m_{Z_d}^{\Delta}\sin(6\omega t) + m_{Z_q}^{\Delta}\cos(6\omega t) & m_{Z_d}^{\Delta}\cos(6\omega t) + m_{Z_q}^{\Delta}\sin(6\omega t) & -m_d^{\Delta}\sin(6\omega t) + m_q^{\Delta}\cos(6\omega t) & m_d^{\Delta}\cos(6\omega t) + m_q^{\Delta}\sin(6\omega t) \\ 0 & 0 & m_{Z_d}^{\Delta}\cos(6\omega t) + m_{Z_q}^{\Delta}\sin(6\omega t) & m_{Z_d}^{\Delta}\sin(6\omega t) - m_{Z_q}^{\Delta}\cos(6\omega t) \end{bmatrix} \tag{48}
$$

These expressions are SSTI if the sixth harmonic components of $\mathcal{H}_{6\omega t}$, from (47), as given in (48), at the top of this page, are neglected.

Finally, replacing (44) and (47) in (46), and further in (42) gives the SSTI dynamics of the circulating current, which can be expressed as

$$
L_{arm}\frac{d\boldsymbol{i}_{dqz}^{\Sigma}}{dt} = \begin{bmatrix} 0 \\ 0 \\ \frac{v_{dc}}{2} \end{bmatrix} - (R_{arm} + \boldsymbol{J}_{-2\omega}L_{arm})\boldsymbol{i}_{dqz}^{\Sigma}
$$
$$
- \frac{1}{4}\begin{bmatrix} 2m_z^{\Sigma} & 0 & 2m_d^{\Sigma} \\ 0 & 2m_z^{\Sigma} & 2m_q^{\Sigma} \\ m_d^{\Sigma} & m_q^{\Sigma} & 2m_z^{\Sigma} \end{bmatrix}\boldsymbol{v}_{Cdqz}^{\Sigma}
$$
$$
- \frac{1}{4}\begin{bmatrix} m_d^{\Delta} + m_{Z_d}^{\Delta} & -m_q^{\Delta} + m_{Z_q}^{\Delta} & m_d^{\Delta} & m_q^{\Delta} \\ -m_q^{\Delta} - m_{Z_q}^{\Delta} & -m_d^{\Delta} + m_{Z_d}^{\Delta} & m_q^{\Delta} & -m_d^{\Delta} \\ m_d^{\Delta} & m_q^{\Delta} & m_{Z_d}^{\Delta} & m_{Z_q}^{\Delta} \end{bmatrix}\boldsymbol{v}_{CdqZ}^{\Delta} \tag{49}
$$

provided the sixth harmonic components are neglected. Notice that the modulated voltages $\boldsymbol{v}_{mdqz}^{\Sigma}$ driving the circulating currents $\boldsymbol{i}_{dqz}^{\Sigma}$ are defined as

$$
\boldsymbol{v}_{mdqz}^{\Sigma} \overset{\text{def}}{=} \frac{1}{4}\begin{bmatrix} 2m_z^{\Sigma} & 0 & 2m_d^{\Sigma} \\ 0 & 2m_z^{\Sigma} & 2m_q^{\Sigma} \\ m_d^{\Sigma} & m_q^{\Sigma} & 2m_z^{\Sigma} \end{bmatrix}\boldsymbol{v}_{Cdq}^{\Sigma}
$$
$$
+ \frac{1}{4}\begin{bmatrix} m_d^{\Delta} + m_{Z_d}^{\Delta} & -m_q^{\Delta} + m_{Z_q}^{\Delta} & m_d^{\Delta} & m_q^{\Delta} \\ -m_q^{\Delta} - m_{Z_q}^{\Delta} & -m_d^{\Delta} + m_{Z_d}^{\Delta} & m_q^{\Delta} & -m_d^{\Delta} \\ m_d^{\Delta} & m_q^{\Delta} & m_{Z_d}^{\Delta} & m_{Z_q}^{\Delta} \end{bmatrix}\boldsymbol{v}_{CdqZ}^{\Delta}. \tag{50}
$$

D. Grid Currents Dynamics

Finally, the derivation of SSTI expressions for the grid current dynamics is presented in the following. The beginning of the proof is the equation for the SSTP dynamics of the grid current in the stationary reference frame from (5) and

(6), recalled in (51a) for convenience. As for the previous cases, the dynamics are rewritten by expressing the *abc* vectors present in (51a) as a function of their *dqz* equivalents, as expressed in (51b)

$$
L_{\text{eq}}^{\text{ac}}\frac{d\boldsymbol{i}_{abc}^{\Delta}}{dt} = \boldsymbol{v}_{mabc}^{\Delta} - \boldsymbol{v}_{abc}^{G} - R_{\text{eq}}^{\text{ac}}\boldsymbol{i}_{abc}^{\Delta}, \tag{51a}
$$

$$
L_{\text{eq}}^{\text{ac}}\frac{d\boldsymbol{P}_{\omega}^{-1}}{dt}\boldsymbol{i}_{dqz}^{\Delta} + L_{\text{eq}}^{\text{ac}}\boldsymbol{P}_{\omega}^{-1}\frac{d\boldsymbol{i}_{dqz}^{\Delta}}{dt}
$$
$$
= \boldsymbol{P}_{\omega}^{-1}\boldsymbol{v}_{mdqz}^{\Delta} - \boldsymbol{P}_{\omega}^{-1}\boldsymbol{v}_{dqz}^{G} - R_{\text{eq}}^{\text{ac}}\boldsymbol{P}_{\omega}^{-1}\boldsymbol{i}_{dqz}^{\Delta}. \tag{51b}
$$

Multiplying (51b) by $\boldsymbol{P}_{\omega}$ and solving for $d\boldsymbol{i}_{dqz}^{\Delta}/dt$ gives

$$
L_{\text{eq}}^{\text{ac}}\frac{d\boldsymbol{i}_{dqz}^{\Delta}}{dt} = \boldsymbol{v}_{mdqz}^{\Delta} - \boldsymbol{v}_{dqz}^{G} - R_{\text{eq}}^{\text{ac}}\boldsymbol{i}_{dqz}^{\Delta} - L_{\text{eq}}^{\text{ac}}\boldsymbol{J}_{\omega}\boldsymbol{i}_{dqz}^{\Delta} \tag{52}
$$

where $\boldsymbol{v}_{dqz}^{G} = [v_d^{G}\ v_q^{G}\ 0]^{\top}$, $\boldsymbol{v}_{mdqz}^{\Delta} \overset{\text{def}}{=} \boldsymbol{P}_{\omega}\boldsymbol{v}_{mabc}^{\Delta}$ and $\boldsymbol{v}_{mabc}^{\Delta}$ is defined in (6). Nonetheless, $\boldsymbol{v}_{mdqz}^{\Delta}$ needs to be assessed in order to verify if (52) produces an SSTI solution. For this purpose, $\boldsymbol{v}_{mdqz}^{\Delta}$ is rewritten by introducing into its definition the expressions for the *a*bc vectors as a function of their *dqz* equivalents, yielding

$$
\boldsymbol{v}_{mdqz}^{\Delta} \overset{\text{def}}{=} -\boldsymbol{P}_{\omega}\frac{1}{2}\big(\boldsymbol{P}_{\omega}^{-1}\boldsymbol{m}_{dqz}^{\Delta} \circ \boldsymbol{P}_{-2\omega}^{-1}\boldsymbol{v}_{Cdqz}^{\Sigma}
$$
$$
+ \boldsymbol{P}_{-2\omega}^{-1}\boldsymbol{m}_{dqz}^{\Sigma} \circ \boldsymbol{P}_{\omega}^{-1}\boldsymbol{v}_{Cdqz}^{\Delta}\big)
$$
$$
\boldsymbol{v}_{mdqz}^{\Delta} \overset{\text{def}}{=} \boldsymbol{M}_{\Psi_B}^{\Delta}\begin{bmatrix} v_{Cd}^{\Sigma} \\ v_{Cq}^{\Sigma} \\ v_{Cz}^{\Sigma} \end{bmatrix} + \boldsymbol{M}_{\Psi_C}^{\Delta}\begin{bmatrix} v_{Cd}^{\Delta} \\ v_{Cq}^{\Delta} \\ v_{Cz}^{\Delta} \end{bmatrix} \tag{53}
$$

where $\boldsymbol{M}_{\Psi_B}^{\Delta}$ and $\boldsymbol{M}_{\Psi_C}^{\Delta}$ are expressed in (54) and (55), as shown at the bottom of the next page, respectively. Both these matrices include nonnegligible third-order harmonic components preventing the possibility of considering SSTI solutions from (52). As in the previous section, it is necessary to replace into (54), (55) and (53) the definitions of m_z^{Δ} and v_{Cz}^{Δ} from (19) and (29), respectively. By this, the modulated

voltage v_{mdqz}^{Δ} can be expressed as

$$v_{mdqz}^{\Delta} = M_{\Psi_B}^{\Delta\star} \begin{bmatrix} v_{Cd}^{\Sigma} \\ v_{Cq}^{\Sigma} \\ v_{Cz}^{\Sigma} \end{bmatrix} + M_{\Psi_C}^{\Delta\star} \begin{bmatrix} v_{Cd}^{\Delta} \\ v_{Cq}^{\Delta} \\ v_{CZ_d}^{\Delta} \\ v_{CZ_q}^{\Delta} \end{bmatrix} \tag{56}$$

where $M_{\Psi_B}^{\Delta\star}$ and $M_{\Psi_C}^{\Delta\star}$ are given in (57) and (58), as shown at the bottom of this page, and the *dq* components will result in SSTI solutions if the sixth harmonic components are neglected.

Replacing the *dq* components from (57) and (58) in (56) and further in (52), and neglecting the sixth harmonic components, gives the SSTI dynamics of the grid current as:

$$L_{eq}^{ac} \frac{di_{dq}^{\Delta}}{dt} = -v_{dq}^{G} - (R_{eq}^{ac} + J_{\omega}L_{eq}^{ac})i_{dq}^{\Delta}$$
$$+ \begin{bmatrix} -m_d^{\Delta} - m_{Z_d}^{\Delta} & m_q^{\Delta} + m_{Z_q}^{\Delta} & -2m_d^{\Delta} \\ m_q^{\Delta} - m_{Z_q}^{\Delta} & m_d^{\Delta} - m_{Z_d}^{\Delta} & -2m_q^{\Delta} \end{bmatrix} v_{Cdqz}^{\Sigma}$$
$$+ \begin{bmatrix} -m_d^{\Sigma} - 2m_z^{\Sigma} & m_q^{\Sigma} & -m_d^{\Sigma} & m_q^{\Sigma} \\ m_q^{\Sigma} & m_d^{\Sigma} - 2m_z^{\Sigma} & -m_q^{\Sigma} & -m_d^{\Sigma} \end{bmatrix} v_{CdqZ}^{\Delta}.$$
$$\tag{59}$$

For the sake of completeness, the SSTI formulation of the zero sequence component of v_{mdqz}^{Δ} from (56) is also defined

in the following. The time-varying signal v_{mz}^{Δ} from (56) is first rewritten as

$$v_{mz}^{\Delta} = v_{mZ_d}^{\Delta} \cos(3\omega t) + v_{mZ_q}^{\Delta} \sin(3\omega t) \tag{60}$$

where the expressions of $v_{mZ_d}^{\Delta}$ and $v_{mZ_q}^{\Delta}$ are given as

$$v_{mZ_d}^{\Delta} = \frac{1}{4}\left(-m_d^{\Delta}v_{Cd}^{\Sigma} - m_q^{\Delta}v_{Cq}^{\Sigma} - 2m_{Z_d}^{\Delta}v_{Cz}^{\Sigma}\right)$$
$$+ \frac{1}{4}\left(-m_d^{\Sigma}v_{Cd}^{\Delta} - m_q^{\Sigma}v_{Cq}^{\Delta} - 2m_z^{\Sigma}v_{CZ_d}^{\Delta}\right) \tag{61a}$$

$$v_{mZ_q}^{\Delta} = \frac{1}{4}\left(-m_q^{\Delta}v_{Cd}^{\Sigma} + m_d^{\Delta}v_{Cq}^{\Sigma} - 2m_{Z_q}^{\Delta}v_{Cz}^{\Sigma}\right)$$
$$+ \frac{1}{4}\left(m_q^{\Sigma}v_{Cd}^{\Delta} - m_d^{\Sigma}v_{Cq}^{\Delta} - 2m_z^{\Sigma}v_{CZ_q}^{\Delta}\right). \tag{61b}$$

Since the variables of (60) oscillate at 3ω in steady state, a similar approach as in Section III-A-3 is used; i.e., an auxiliary virtual variable $v_{mZ\beta}^{\Delta}$, which is 90° phase-shifted from v_{mz}^{Δ} (renamed $v_{mZ\alpha}^{\Delta}$ for convenience) is created. This is obtained by replacing the $\sin(3\omega t)$ and $\cos(3\omega t)$ that appear in (60) by $\sin(3\omega t)$ and $-\cos(3\omega t)$, respectively, as given by

$$v_{mZ_\alpha}^{\Delta} = v_{mZ_d}^{\Delta} \cos(3\omega t) + v_{mZ_q}^{\Delta} \sin(3\omega t) \tag{62a}$$
$$v_{mZ_\beta}^{\Delta} = v_{mZ_d}^{\Delta} \sin(3\omega t) - v_{mZ_q}^{\Delta} \cos(3\omega t). \tag{62b}$$

$$M_{\Psi_B}^{\Delta} = \frac{1}{4} \left[\begin{array}{ccc} -m_d^{\Delta} - 2m_z^{\Delta}\cos(3\omega t) & m_q^{\Delta} + 2m_z^{\Delta}\sin(3\omega t) & -2m_d^{\Delta} \\ m_q^{\Delta} - 2m_z^{\Delta}\sin(3\omega t) & m_d^{\Delta} - 2m_z^{\Delta}\cos(3\omega t) & -2m_q^{\Delta} \\ \hdashline -m_d^{\Delta}\cos(3\omega t) - m_q^{\Delta}\sin(3\omega t) & m_d^{\Delta}\sin(3\omega t) - m_q^{\Delta}\cos(3\omega t) & -2m_z^{\Delta} \end{array} \right] \tag{54}$$

$$M_{\Psi_C}^{\Delta} = \frac{1}{4} \left[\begin{array}{ccc} -m_d^{\Sigma} - 2m_z^{\Sigma} & m_q^{\Sigma} & -2m_d^{\Sigma}\cos(3\omega t) + 2m_q^{\Sigma}\sin(3\omega t) \\ m_q^{\Sigma} & m_d^{\Sigma} - 2m_z^{\Sigma} & -2m_q^{\Sigma}\cos(3\omega t) - 2m_d^{\Sigma}\sin(3\omega t) \\ \hdashline m_q^{\Sigma}\sin(3\omega t) - m_d^{\Sigma}\cos(3\omega t) & -m_q^{\Sigma}\cos(3\omega t) - m_d^{\Sigma}\sin(3\omega t) & -2m_z^{\Sigma} \end{array} \right] \tag{55}$$

$$M_{\Psi_B}^{\Delta\star} = \frac{1}{4} \left[\begin{array}{ccc} -m_d^{\Delta} - m_{Z_d}^{\Delta} & m_q^{\Delta} + m_{Z_q}^{\Delta} & -2m_d^{\Delta} \\ m_q^{\Delta} - m_{Z_q}^{\Delta} & m_d^{\Delta} - m_{Z_d}^{\Delta} & -2m_q^{\Delta} \\ \hdashline -m_d^{\Delta}\cos(3\omega t) - m_q^{\Delta}\sin(3\omega t) & m_d^{\Delta}\sin(3\omega t) - m_q^{\Delta}\cos(3\omega t) & -2m_{Z_d}^{\Delta}\cos(3\omega t) - 2m_{Z_q}^{\Delta}\sin(3\omega t) \end{array} \right]$$
$$+ \underbrace{\begin{bmatrix} -m_{Z_d}^{\Delta}\cos(6\omega t) - m_{Z_q}^{\Delta}\sin(6\omega t) & m_{Z_d}^{\Delta}\sin(6\omega t) - m_{Z_q}^{\Delta}\cos(6\omega t) & 0 \\ m_{Z_q}^{\Delta}\cos(6\omega t) - m_{Z_d}^{\Delta}\sin(6\omega t) & -m_{Z_q}^{\Delta}\sin(6\omega t) - m_{Z_d}^{\Delta}\cos(6\omega t) & 0 \\ \hdashline 0 & 0 & 0 \end{bmatrix}}_{\approx 0} \tag{57}$$

$$M_{\Psi_C}^{\Delta\star} = \frac{1}{4} \left[\begin{array}{cccc} -m_d^{\Sigma} - 2m_z^{\Sigma} & m_q^{\Sigma} & -m_d^{\Sigma} & m_q^{\Sigma} \\ m_q^{\Sigma} & m_d^{\Sigma} - 2m_z^{\Sigma} & -m_q^{\Sigma} & -m_d^{\Sigma} \\ \hdashline m_q^{\Sigma}\sin(3\omega t) - m_d^{\Sigma}\cos(3\omega t) & -m_q^{\Sigma}\cos(3\omega t) - m_d^{\Sigma}\sin(3\omega t) & -2m_z^{\Sigma}\cos(3\omega t) & -2m_z^{\Sigma}\sin(3\omega t) \end{array} \right]$$
$$+ \underbrace{\begin{bmatrix} 0 & 0 & m_q^{\Sigma}\sin(6\omega t) - m_d^{\Sigma}\cos(6\omega t) & -m_q^{\Sigma}\cos(6\omega t) - m_d^{\Sigma}\sin(6\omega t) \\ 0 & 0 & -m_q^{\Sigma}\cos(6\omega t) - m_d^{\Sigma}\sin(6\omega t) & -m_q^{\Sigma}\sin(6\omega t) + m_d^{\Sigma}\cos(6\omega t) \\ \hdashline 0 & 0 & 0 & 0 \end{bmatrix}}_{\approx 0} \tag{58}$$
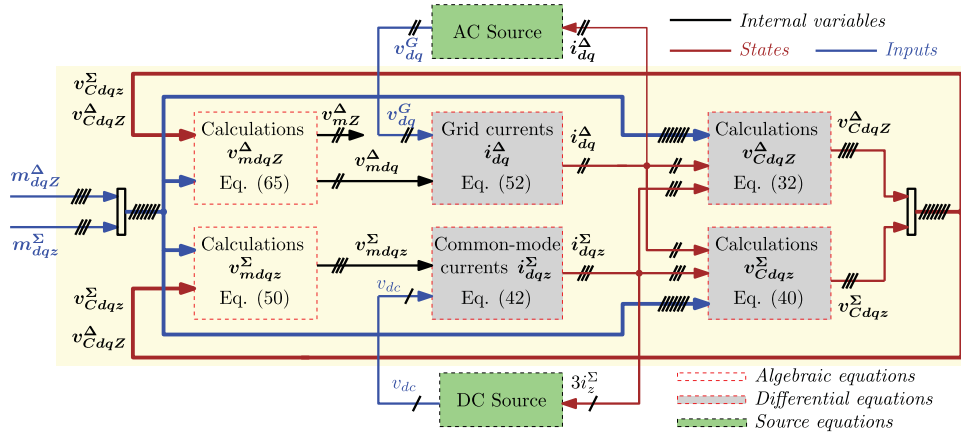
Fig. 4.   Summary of the MMC equations in dqz frame.

 Furthermore, (62) is written in vector form as in (63), with the definitions given in (64) and with the rotational transformation $T_{3\omega}$ defined in (25)

$$v^{\Delta}_{mZ_{\alpha\beta}} = T^{-1}_{3\omega}v^{\Delta}_{mZ}, \tag{63}$$

$$v^{\Delta}_{mZ_{\alpha\beta}} \stackrel{\text{def}}{=} [v^{\Delta}_{mZ_\alpha}; v^{\Delta}_{mZ_\beta}]^\top; \quad v^{\Delta}_{mZ} \stackrel{\text{def}}{=} [v^{\Delta}_{mZ_d}; v^{\Delta}_{mZ_q}]^\top. \tag{64}$$

Finally, an extended definition of the modulated voltage difference is introduced as $v^{\Delta}_{mdqZ} \stackrel{\text{def}}{=} [v^{\Delta}_{md}\ v^{\Delta}_{mq}\ v^{\Delta}_{mZ_d}\ v^{\Delta}_{mZ_q}]^\top$ and is expressed as

$$v^{\Delta}_{mdqZ} = \begin{bmatrix} -m^{\Delta}_d - m^{\Delta}_{Z_d} & m^{\Delta}_q + m^{\Delta}_{Z_q} & -2m^{\Delta}_d \\ m^{\Delta}_q - m^{\Delta}_{Z_q} & m^{\Delta}_d - m^{\Delta}_{Z_d} & -2m^{\Delta}_q \\ \hdashline -m^{\Delta}_d & -m^{\Delta}_q & -2m^{\Delta}_{Z_d} \\ -m^{\Delta}_q & m^{\Delta}_d & -2m^{\Delta}_{Z_q} \end{bmatrix} \begin{bmatrix} v^{\Sigma}_{Cd} \\ v^{\Sigma}_{Cq} \\ v^{\Sigma}_{Cz} \end{bmatrix} +$$

$$\begin{bmatrix} -m^{\Sigma}_d - 2m^{\Sigma}_z & m^{\Sigma}_q & -m^{\Sigma}_d & m^{\Sigma}_q \\ m^{\Sigma}_q & m^{\Sigma}_d - 2m^{\Sigma}_z & -m^{\Sigma}_q & -m^{\Sigma}_d \\ \hdashline -m^{\Sigma}_d & -m^{\Sigma}_q & -2m^{\Sigma}_z & 0 \\ m^{\Sigma}_q & -m^{\Sigma}_d & 0 & -2m^{\Sigma}_z \end{bmatrix} \begin{bmatrix} v^{\Delta}_{Cd} \\ v^{\Delta}_{Cq} \\ v^{\Delta}_{CZ_d} \\ v^{\Delta}_{CZ_q} \end{bmatrix}. \tag{65}$$

E. Summary of MMC Model With SSTI Solution

As a result of the presented derivations, the MMC SSTI dynamics can be represented by the differential equations in (32), (40), (49), and (59), corresponding to the 12 SSTI state variables of the arm voltages difference v^{Δ}_{CdqZ}, arm voltages sum v^{Σ}_{Cdqz}, circulating currents i^{Σ}_{dqz}, and grid currents i^{Δ}_{dq}. Moreover, the model assumes seven SSTI control inputs, represented by the sum and difference of the modulation indices m^{Σ}_{dqz} and m^{Δ}_{dqZ}. The modulated voltages v^{Δ}_{mdqZ} and v^{Σ}_{mdqz} are expressed by the algebraic equations given in (65) and (50), respectively. In addition, the model receives three physical SSTI inputs represented by the voltage at the dc terminals v_{dc} and the dq components of the grid voltage, v^{G}_{dq}. Finally, the proposed MMC model with SSTI solution is graphically represented in Fig. 4.

This presented model is generally valid for SSTI representation of the MMC, independently of how the time-invariant components of the modulation signals m^{Σ}_{dqz} and m^{Δ}_{dqZ} are

obtained. Thus, the model can be combined with any control system that can be modeled by SSTI equations as, for instance, utilized in [36], [39], and [42]. Thus, the model can also provide a detailed representation of the internal dynamics of MMCs with CM-based control. However, as shown in [43], an SSTI representation of cases with CM-based control can be more easily obtained from $\Sigma\Delta$ energy-based modeling of the internal voltage dynamics.

IV. MODEL VALIDATION BY TIME-DOMAIN SIMULATION

To validate the developed modeling approach, the results from time-domain simulation of the following three different models are shown and discussed in this section.

1) The proposed time-invariant MMC model from Fig. 4 as derived in Section III, representing the SSTI dynamics of the arm voltages difference, arm voltages sum, circulating currents, and grid currents. The simulations result obtained with this model are identified in the figure legends by a ⋆ symbol as a superscript for each variable.

2) The AAM of a three-phase MMC, where each arm is represented by a controlled voltage source and where the internal arm voltage dynamics is represented by an equivalent arm capacitance as indicated in the lower right part of Fig. 2 [4], [5], [13]. This model includes nonlinear effects except for the switching operations and the dynamics of the SM capacitor voltage balancing algorithm, as indicated in Fig. 1. The model is simulated in Matlab/Simulink with the SimPowerSystem toolbox. The simulation results obtained with this model are identified in figure legends by "AAM."

3) An electromagnetic transient (EMT) simulation implemented in EMTP-RV of an MMC having 400 SMs per arm, with a capacitance of $0.01302F$ each. The MMC is modeled with the so-called "Model # 2: Equivalent Circuit-Based Model" from [40]. This model includes nonlinear effects, the switching operations and the dynamics of the SM capacitor voltage balancing algorithm from [33], as indicated in Fig. 1. The simulation results obtained with this model are identified in figure legends by "EMT."
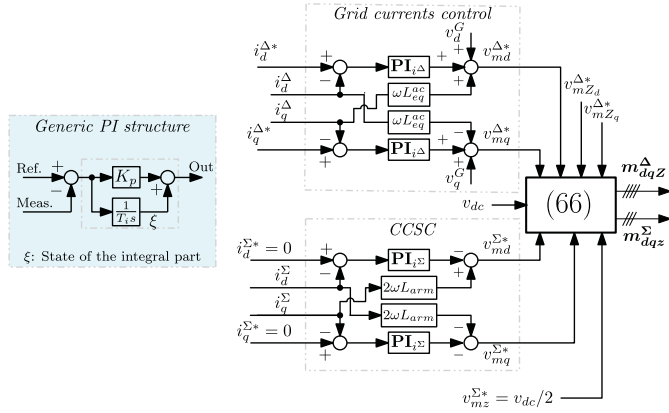
Fig. 5. CCSC and standard SRRF grid current vector control.

All the simulations are based on the MMC HVDC single-terminal configuration shown in Fig. 2, with the parameters given in Table II in the Appendix. The MMC is operated with the well-known CCSC technique described in [33], and with standard SRRF vector control for the grid current, similar to the case analyzed in [31]. The modulation index input signals for the time-invariant MMC model are calculated directly from the voltage references resulting from the conventional control loops according to

$$
\begin{bmatrix} m_{dqZ}^{\Delta} \\ m_{dqz}^{\Sigma} \end{bmatrix} = \frac{2}{v_{dc}} \begin{bmatrix} -I_{4\times 4} & 0_{4\times 3} \\ 0_{3\times 4} & I_{3\times 3} \end{bmatrix} \begin{bmatrix} v_{mdqZ}^{\Delta *} \\ v_{mdqz}^{\Sigma *} \end{bmatrix} \tag{66}
$$

where $I_{n\times m}$ is the identity $n \times m$ matrix. This strategy for calculation of the insertion indices is referred to as "uncompensated modulation" (UCM) [31]. The resulting control structure providing the modulation signal inputs to the developed MMC model is shown in Fig. 5. For comparing the simulated models, it should be considered that the AAM and EMT reference models are conventional stationary frame models of a three-phase MMC, while the derived model with SSTI solution represents the MMC dynamics by variables transformed into a set of SRRFs. Nonetheless, comparison of transient and steady-state response is simpler when the variables have SSTI representation. Thus, in most cases, the results obtained from the reference model are transformed into the appropriate SRRFs to ease the comparison. However, the results from the models with SSTI solution can also be transformed to the stationary phase coordinates, as will be demonstrated by an example. All the results are plotted in per unit quantities.

It is also worth mentioning that the verification of the scientific contribution represented by the proposed modeling approach should be done first and foremost with respect to the model it has been derived from, i.e., the AAM. This initial comparison, where the AAM is considered as the reference model, is the most important for evaluating the accuracy of the proposed modelling approach and the impact of the simplifications introduced as part of the presented derivations. Thus, the analysis of simulation results that will follow is mainly focused on the SSTI *dqz* model and the AAM. Nonetheless, for a more practical-oriented comparison, the results from the "EMT" model have been included in the figures, to indicate
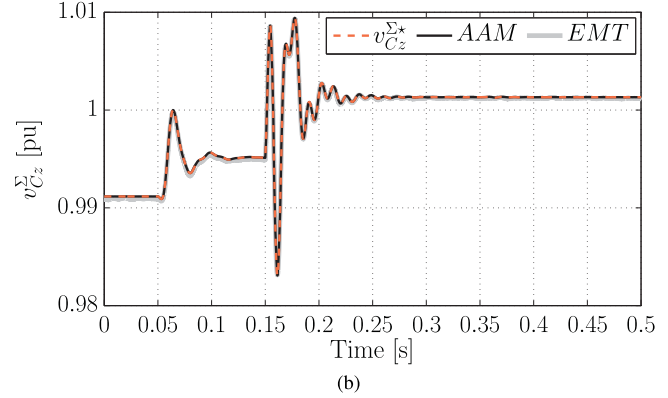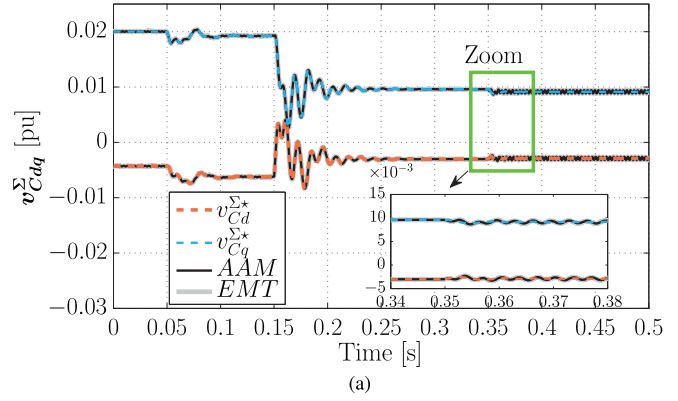

Fig. 6. Comparison of the derived SSTI model with the AAM and EMT models: arm capacitor voltage sum. (a) *dq* components. (b) Zero sequence.

the accuracy of the proposed modeling approach, as well as the AAM, with respect to a detailed switching model of the MMC.

To excite the MMC dynamics in the different models, first a step of the ac-side reactive current reference corresponding to a step of reactive power flow from zero to -0.1 p.u. is introduced at $t = 0.05\ s$. Second, the ac-side active current reference is changed in a step corresponding to a reduction of the active power reference from 1 to 0.5 p.u. at $t = 0.15\ s$. Finally, the zero sequence modulated voltage reference $v_{mZ_d}^{\Delta *}$ is changed from 0 to 0.02 p.u. at $t = 0.35\ s$, and at the same time $v_{mZ_q}^{\Delta *}$ is changed from 0 to -0.01 p.u.

The dynamic response of the voltage sum variables v_{Cdqz}^{Σ} for the simulated scenario are illustrated in Fig. 6. More precisely, the *dq* components of this variable are given in Fig. 6(a), while its zero sequence component is shown in Fig. 6(b). From the curves in Fig. 6, it can be seen how the results from the AAM used as reference, as well as from the detailed EMT model, are practically identical to the results from the model with the SSTI solution derived in this paper. This is true for both transient and steady-state conditions. Notice that the steady-state value of v_{Cz}^{Σ} changes with respect to each of the reference steps, as the use of the CCSC implies that there is no closed-loop regulation of the capacitive energy stored in the MMC. Furthermore, the nonzero steady-state values of v_{Cdq}^{Σ} reflect the 2ω oscillations that this variable has in the stationary *abc* reference frame. It can also be noticed that the perturbation introduced at $t = 0.35\ s$ is
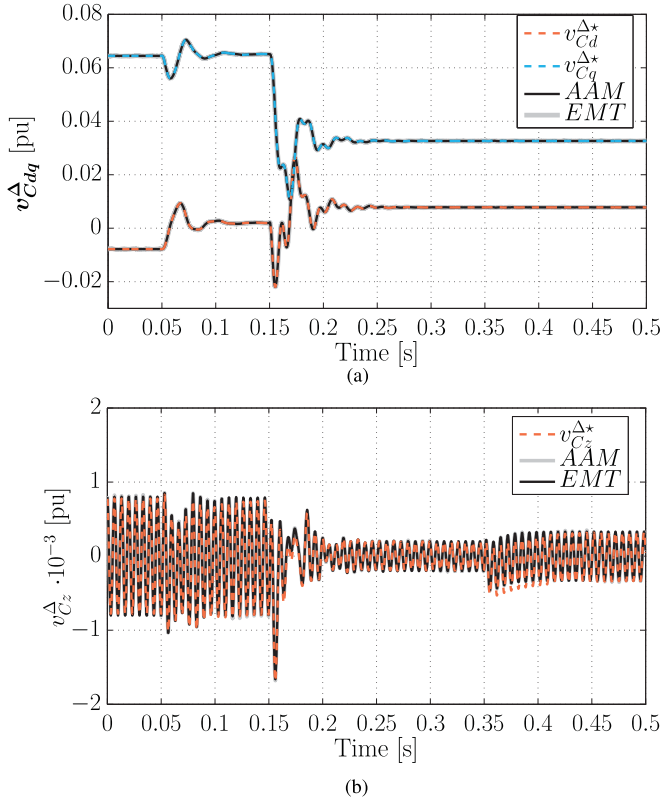
Fig. 7.   Comparison of the derived SSTI model with the AAM and EMT models: arm capacitor voltage difference. (a) dq components. (b) Zero sequence component transformed to scalar, time-periodic, representation.

Fig. 8.   SSTI representation of the voltage difference zero sequence.

slightly increasing the 6ω oscillations in v_{Cdq}^{Σ} of the reference AAM- and EMT-models. As expected, the SSTI model only manages to capture accurately the average dynamics after this perturbation, since the 6ω components have been neglected in the derivation of the model.

The dynamics of the energy difference variables v_{Cdqz}^{Δ} are depicted in Fig. 7. More precisely, Fig. 7(a) illustrates the behavior of the dq components during the simulated scenario, while Fig. 7(b) shows the results for the zero sequence component. In terms of accuracy, both of the subfigures show how the proposed model with SSTI solution accurately captures the behavior of the AAM- and EMT-MMC models used as reference. This is particularly true for the case of v_{Cdq}^{Δ} as almost no distinction can be made between the voltage waveforms resulting from the models. For v_{Cz}^{Δ}, however, it is possible to notice a slight mismatch between the derived model and the AAM, particularly during the transient behavior between $t = 0.15\ s$ and $t = 0.2\ s$ and between $t = 0.35\ s$ and $t = 0.4\ s$. This is indeed associated with the neglected sixth harmonic components in the mathematical derivation of the proposed model with SSTI solution. Nonetheless, the error is very small and does not have a noticeable influence on the general dynamics of the model.

Notice that the comparison between the reference models and the proposed MMC model with SSTI solution in Fig. 7 has been presented using the SSTP signal v_{Cz}^{Δ} instead of its equivalent SSTI version v_{CZ}^{Δ} defined in Section III. This is
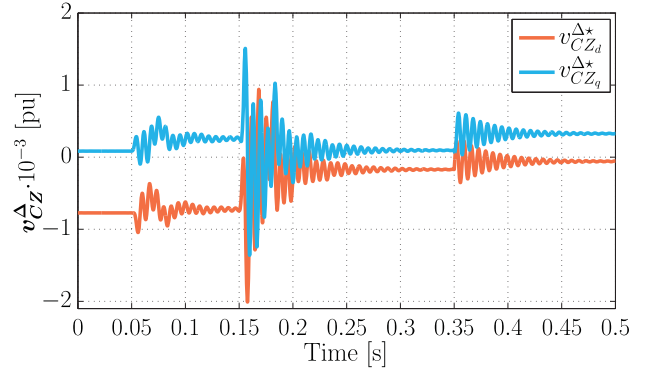
done for simplicity, as the dynamics of the virtual system used to create v_{CZ}^{Δ} do not directly exist in the reference AAM-MMC model. However, for the sake of completeness, the dynamics of the SSTI v_{CZ}^{Δ} in the 3ω SRRF as obtained with the proposed model are depicted in Fig. 8, where it can be confirmed that both the $v_{CZ_d}^{\Delta}$ and $v_{CZ_q}^{\Delta}$ variables reach a constant value in steady-state operation.

As already stated, it is always possible to reconstruct the SSTP variables in the abc stationary frame and in upper U and lower L arm coordinates from the SSTI dqz variables in their $\Sigma-\Delta$ representation. For example, consider the SSTI variables v_{Cdqz}^{Σ} and v_{CdqZ}^{Δ} that result from the proposed modeling approach, as plotted in Figs. 6–8. From these variables it is possible to reconstruct the natural MMC SSTP variables v_{Cabc}^{U} and v_{Cabc}^{L} using the fact that $v_{Cabc}^{\Sigma} = P_{-2\omega}^{-1} v_{Cdqz}^{\Sigma}$, $v_{Cabc}^{\Delta} = P_{\omega}^{-1}[v_{Cd}^{\Delta}; v_{Cq}^{\Delta}; (v_{CZ_d}^{\Delta}\cos(3\omega t) + v_{CZ_q}^{\Delta}\sin(3\omega t))]^{\top}$, $v_{Cabc}^{U} = v_{Cabc}^{\Sigma} + v_{Cabc}^{\Delta}$, and $v_{Cabc}^{L} = v_{Cabc}^{\Sigma} - v_{Cabc}^{\Delta}$. The result of this calculation is shown in the upper part of Fig. 9, where v_{Ca}^{U} and v_{Ca}^{L} calculated from the derived model are compared with the total (summed) upper and lower arm capacitor voltages of the EMT model, yielding in an accurate match. Furthermore, the zoomed plot in the lower part of Fig. 9 emphasizes the behavior close to the step at $t = 0.15\ s$, and also shows the voltages of the first 10 SMs (out of the 400) present in the EMT model. This figure shows that even if the individual SMs voltages of each arm are not identical, the aggregate voltage $v_C^{U,L}$ for an MMC with high number of levels can be accurately represented by the proposed SSTI modeling approach.[1]

The dynamics of the circulating currents i_{dqz}^{Σ} are shown in Fig. 10, where Fig. 10(a) depicts the dynamics of the dq components. Fig. 10(b) shows the zero sequence component multiplied by three, since this signal corresponds to the dc current i_{dc} flowing into the dc terminals of the MMC. From the figure it can also be concluded that the proposed model with SSTI solution replicates quite accurately the current dynamics of the reference models. It can be noticed that the accuracy of the model is very good for the zero sequence component i_z^{Σ}. However, for the dq component, it is possible to notice the effect of neglecting the sixth-order harmonics in the SSTI

[1]This is as expected, and is confirmed with a similar accuracy as demonstrated for the SSTP AAM model in [40].
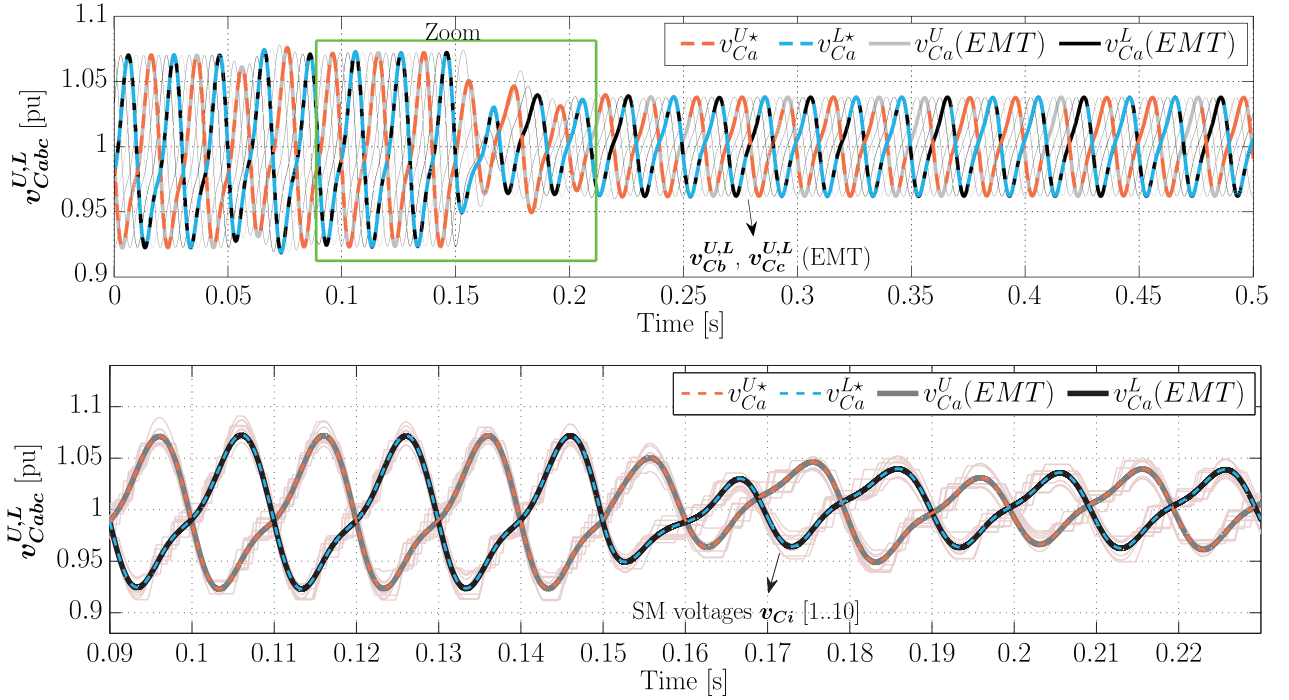
Fig. 9.   Comparison between the derived SSTI model and the AAM and EMT models in the stationary phase coordinates: capacitor voltage sum of the upper and lower arms.
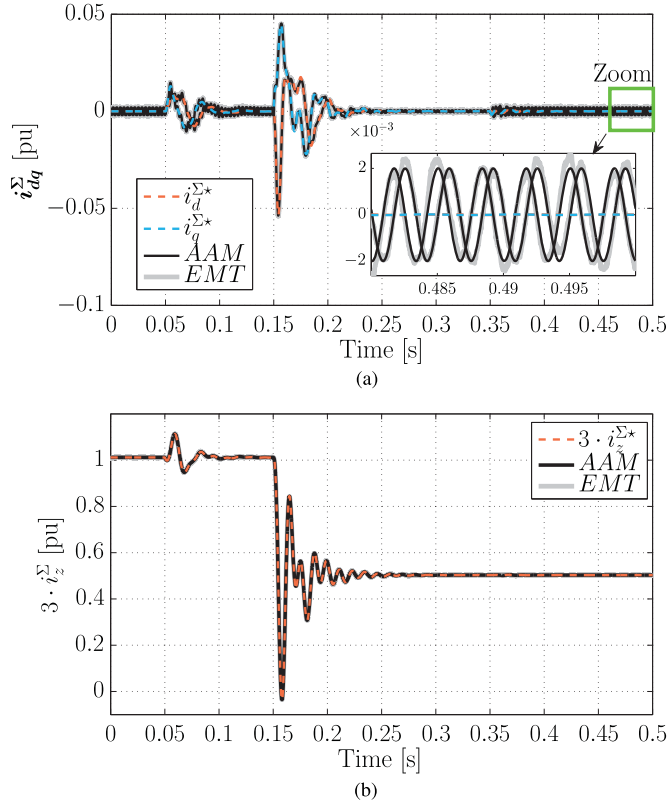

Fig. 10.   Comparison of the derived SSTI model with the AAM and EMT models: circulating current. (a) *dq* components. (b) Zero sequence.

Fig. 11.   Comparison of the proposed SSTI model with the AAM and EMT models: grid current *dq* components.

average value of the 6ω current components. An example of how the sixth harmonic oscillations appear as superimposed to the average dynamics of the presented SSTI model is shown in the zoomed-in view of the steady-state operation of i_{dq}^{Σ} depicted in the small plot inside Fig. 10. Interestingly, a mismatch between the AAM and the EMT models is also observed in these variables, due to the discontinuous switching effects that have been neglected in the AAM and SSTI models.

Finally, the dynamics of the *dq* components of the grid current are shown in Fig. 11. It can be seen that for these variables, the results from the reference models and from the derived model with SSTI characteristics are practically identical.

V. EXAMPLE OF LINEARIZATION AND EIGENVALUE ANALYSIS

As mentioned in the Introduction, one of the main advantages of the obtained MMC model with SSTI solution,

model. Although these components are very small, they are present in the reference AAM and EMT MMC models, and can be noticed in the curves. Yet, the proposed model captures most of the current dynamics, and accurately represents the
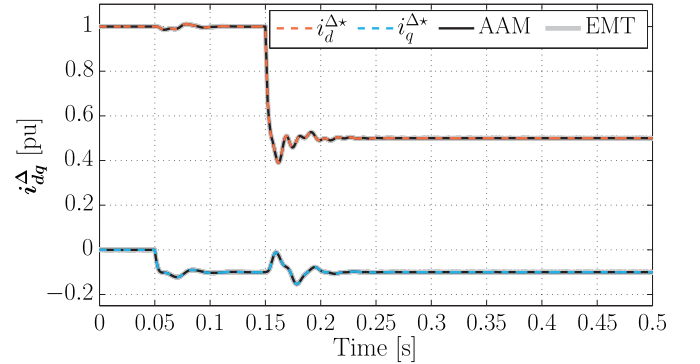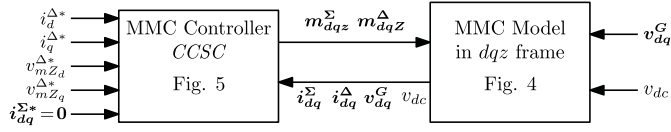
Fig. 12.   Block diagram of SSTI equations for linearization.

compared to SSTP models, is that it can be linearized and interfaced with larger system models for eigenvalue-based analysis of stability and small-signal dynamics. For presenting an example of such linearization and eigenvalue analysis, the nonlinear time-invariant (NTI) model presented in Section III and a corresponding model of the control system from Section IV are first interconnected as shown in Fig. 12. This interconnected model is represented by a subset of ordinary differential equations $\boldsymbol{f}$ expressed as

$$\dot{\boldsymbol{x}}(t) = \boldsymbol{f}\left(\boldsymbol{x}(t), \boldsymbol{u}(t)\right) \tag{67}$$

where $\boldsymbol{x}$ represents the states of the system as defined by

$$\boldsymbol{x} = \left[\underbrace{\boldsymbol{\xi}_{i_{dq}^{\Delta}}^{\top} \boldsymbol{\xi}_{i_{dq}^{\Sigma}}^{\top}}_{\text{Controllers}} \underbrace{\boldsymbol{i}_{dq}^{\Delta}{}^{\top} \boldsymbol{i}_{dqz}^{\Sigma}{}^{\top} \boldsymbol{v}_{Cdqz}^{\Sigma}{}^{\top} \boldsymbol{v}_{CdqZ}^{\Delta}{}^{\top}}_{\text{MMC}}\right]^{\top} \in \Re^{16} \tag{68}$$

and $\boldsymbol{u}$ represents the inputs as defined by

$$\boldsymbol{u} = \left[\underbrace{i_d^{\Delta*} i_q^{\Delta*} v_{mZ_d}^{\Delta*} v_{mZ_q}^{\Delta*} i_d^{\Sigma*} i_q^{\Sigma*}}_{\text{Control Inputs}} \underbrace{v_d^G v_q^G v_{dc}}_{\text{System Inputs}}\right]^{\top} \in \Re^9. \tag{69}$$

The nonlinear model from (67) can be linearized around a steady-state operating point by means of the Jacobian linearization method [8], [22], [44], resulting in an LTI representation expressed as

$$\Delta\dot{\boldsymbol{x}}(t) = \boldsymbol{A}(\boldsymbol{x_0}, \boldsymbol{u_0})\Delta\boldsymbol{x}(t) + \boldsymbol{B}(\boldsymbol{x_0}, \boldsymbol{u_0})\Delta\boldsymbol{u}(t). \tag{70}$$

Thus, each element A_{ij} and B_{ij} of the matrices $\boldsymbol{A}$ and $\boldsymbol{B}$ are related to the equations $\boldsymbol{f}$ as

$$A_{ij} = \left.\frac{\partial f_i(\boldsymbol{x}, \boldsymbol{u})}{\partial x_j}\right|_{(\boldsymbol{x_0}; \boldsymbol{u_0})}; \quad B_{ij} = \left.\frac{\partial f_i(\boldsymbol{x}, \boldsymbol{u})}{\partial u_j}\right|_{(\boldsymbol{x_0}; \boldsymbol{u_0})}. \tag{71}$$

Any equilibrium point, defined by $(\boldsymbol{x_0}, \boldsymbol{u_0})$, can be calculated by solving the nonlinear system of equations from (67) by setting $\dot{\boldsymbol{x}}(t)$ equal to zero. The obtained LTI model linearized at $(\boldsymbol{x_0}, \boldsymbol{u_0})$ can be used for evaluating small-signal dynamics and stability by eigenvalue analysis.

To validate the small-signal modeling of the MMC and its controller, the results from a time-domain simulation of two different models are shown and discussed in the following. For this validation, the SSTI model is linearized at the operating point defined by ac active and reactive powers equal to 1 and 0 p.u., respectively, and the response is shown for a step of the ac-side active current reference $i_d^{\Delta}*$, corresponding to a step of the ac-side active power of -0.2 p.u. The linearized model is referred to as "LTI" in the legend, while the "EMT" corresponds to the same detailed simulation model
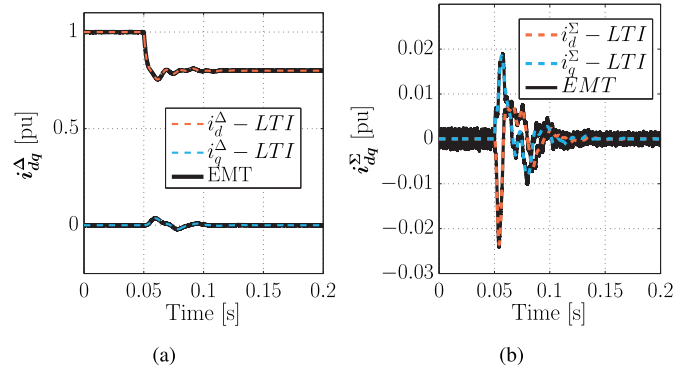

Fig. 13.   LTI time-domain validation. (a) Grid currents. (b) Circulating currents.
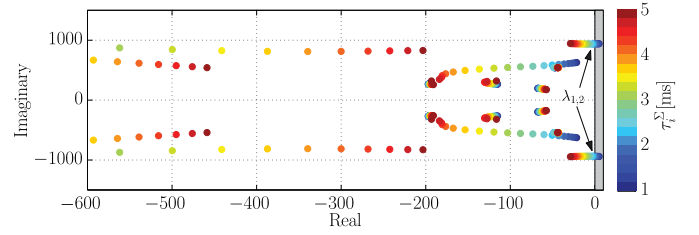

Fig. 14.   Eigenvalue trajectories for variation of CCSC response time τ_i^{Σ}, from 5 to 1 ms.

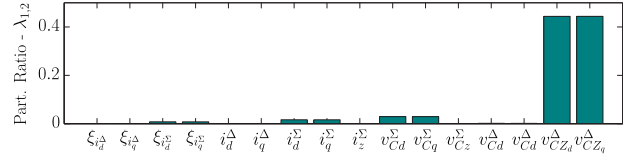Fig. 15.   Participation factors for the eigenvalues $\lambda_{1,2}$—the system parameters are the same as used for Fig. 13.

as used in the previous section. As depicted in Fig. 13, the linearized version of the proposed time-invariant model reproduces accurately the MMC dynamics around a given operating point.

Once the LTI model is validated, the eigenvalues of the $\boldsymbol{A}$ matrix from (70) can be calculated for modal analysis of the MMC to gain insight into the system dynamics. As this section only concerns the application of the proposed model for small-signal stability analysis, the following study is focused on the impact of the tuning of the CCSC on the internal dynamics. In Fig. 14, the trajectory of the eigenvalues is shown for a variation of the response time τ_i^{Σ} of the CCSC, from 5 to 1 ms. As shown in the figure, the pair of eigenvalues $\lambda_{1,2}$ crosses to the right-hand plane when τ_i^{Σ} is decreased, and the system becomes unstable for a fast CCSC with τ_i^{Σ} below approximately 1.5 ms. For understanding the origin of $\lambda_{1,2}$, participation factor analysis is conducted for the system [22]. The absolute values of the participation factors are plotted in Fig. 15 for the same parameters as used in Fig. 13.

The participation factor analysis shows that the potentially unstable eigenvalues $\lambda_{1,2}$ are mostly associated with the zero sequence arm capacitor voltage differences, i.e., $\boldsymbol{v}_{CZdq}^{\Delta}$, but there is also a small contribution from $\boldsymbol{v}_{Cdq}^{\Sigma}$, $\boldsymbol{i}_{dq}^{\Sigma}$, and the integral states $\boldsymbol{\xi}_{i_{dq}^{\Sigma}}$ of the circulating current controllers.
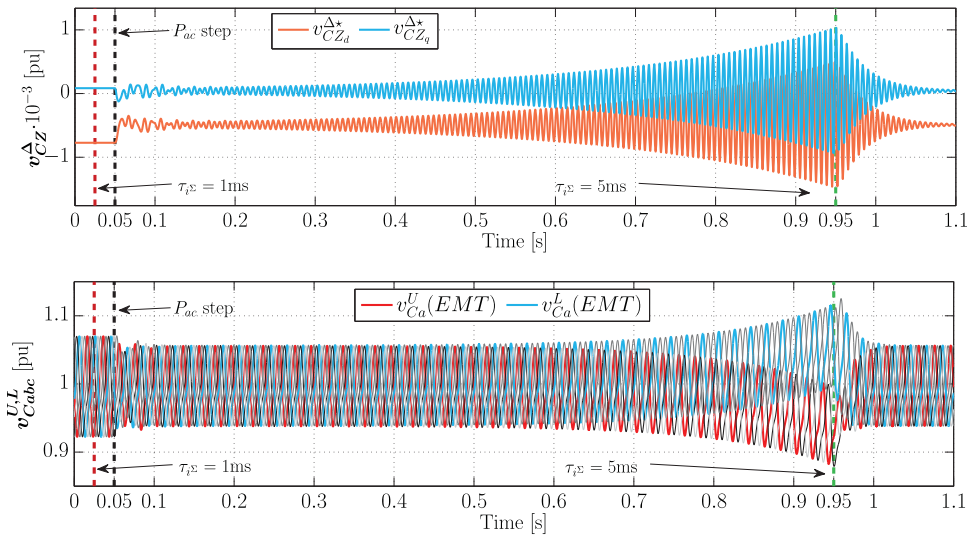
Fig. 16. Time-domain simulation for validating the results from Fig. 14, showing the impact of the CCSC parameters on the stability of the system. Results from the SSTI model (top) and results from the detailed EMT model (bottom) are shown.

With the parameters used for the results in Fig. 15, the imaginary part of $\lambda_{1,2}$ is equal to 937 rad/s, which corresponds to a frequency of 150 Hz. Thus, for an unstable case, this mode should correspond to an exponentially increasing oscillation of 150 Hz in the 3ω SRRF. However, when transformed back into the stationary reference frame by applying (29), this mode should result in an exponentially increasing dc-component of the zero sequence voltage difference v_{Cz}^{Δ}. Thus, the same instability should appear in all aggregated arm voltages of the MMC, with opposite directions for the upper and lower arms.

For demonstrating the unstable behavior predicted by the eigenvalue analysis, the results from a time-domain simulation are presented in Fig. 16, where the upper plot shows the results of v_{CZ}^{Δ} from the "LTI" model and the lower plot shows the arm-capacitor voltages $v_{Cabc}^{U,L}$ of the "EMT" model (in *abc* frame). At $t = 0$ s, the gains of the CCSC controllers are set to obtain a response time of $\tau_i^{\Sigma} = 5$ ms. At $t = 0.025$ s, τ_i^{Σ} is changed to 1 ms, which corresponds to an unstable behavior according to Fig. 14. For perturbing the system, a step of -0.2 pu is applied to the active current reference at $t = 5$ ms. At this point, the instability becomes clearly noticeable. Finally, at $t = 0.95$ s, τ_i^{Σ} is changed back to 5 ms, and the system returns to stable operation. It can also be confirmed from the figures that the instability appears as predicted from the eigenvalue analysis, with an increasing oscillation of $v_{CZ_d}^{\Delta}$ and $v_{CZ_q}^{\Delta}$ in the 3ω SRRF, which reflects in exponentially deviating dc-components of the arm capacitor voltages of the EMT model.

It can be noted that the results presented above are in concordance with the findings in [32]. However, in [32] the linearized model was based on dynamic phasors and harmonic superposition, while the model in this paper is obtained directly from reformulation and SRRF transformation of the dynamic equations of the AAM. Thus, the presented results are mainly intended as a simple verifiable example of how the generalized voltage-based SSTI representation of the MMC developed in this paper can be utilized for linearization and eigenvalue-based analysis of small-signal dynamics.

VI. CONCLUSION

This paper presents a modeling approach for obtaining a state-space representation of an MMC where all variables reach a constant equilibrium in steady-state operation. This was achieved by applying a voltage-current-based $\Sigma-\Delta$ representation, which enabled separation of the MMC variables according to their oscillation frequencies as part of the initial model formulation. A procedure for deriving equivalent time-invariant dqz representations of all state variables by applying three different Park transformations was presented, referring the variables to three different reference frames, rotating at once, twice, and thrice the fundamental grid frequency. The resulting model accurately represents the dynamic coupling between the dominant frequency components appearing within an MMC. The model can also be directly linearized at any feasible operating condition, and allows for accurate eigenvalue-based analysis of the internal dynamics of an MMC.

The presented modeling approach can be considered independent of the modulation and control strategy adopted, as only the physical equations of the MMC have been mathematically manipulated, gaining a more generalized model compared to previous efforts. Thus, the model can be easily expanded with representation of various MMC control strategies. Furthermore, the model can be interconnected with any suitable dynamic models of the ac-side and dc-side system, for detailed small-signal eigenvalue analysis of an individual MMC HVDC terminal, or an HVDC transmission scheme integrated in a larger power system configuration.

The results from a time-domain simulation of an established averaged arm model as well as from a detailed model of an MMC with 400 SMs per arm validate the approach presented in this paper. These results verify how the derived state-space model with SSTI solution accurately captures the MMC internal dynamics while imposing that all the state variables

TABLE II
NOMINAL VALUES AND PARAMETERS (τ_x, ζ_x: RESPONSE
TIME AND DAMPING FOR VARIABLE "x")

U_{1n}	320[kV]	R_f	0.512[Ω]	$\tau_{i\Delta}$	10[ms]
f_n	50[Hz]	L_f	58.7[mH]	$\zeta_{i\Delta}$	0.7[-]
N	400[-]	R_{arm}	1.024[Ω]	$\tau_{i\Sigma}$	5[ms]
C_{arm}	32.55[μF]	L_{arm}	48.9[mH]	$\zeta_{i\Sigma}$	0.7[-]

settle to a constant equilibrium in steady-state operation. The validity of the corresponding linearized model and an example of the results from eigenvalue-based analysis of small-signal stability have also been verified by time-domain simulations.

Further utilization and extension of the presented modeling approach can enable a wide range of studies related to analysis and control system design for MMCs. As the derived model can be linearized, it can be utilized for studies of various multivariable control techniques and optimization methods. Since the developed MMC model with SSTI dynamics preserves the mathematical information about system nonlinearities, it is also suited for application of techniques for multivariable nonlinear analysis and control.

APPENDIX

The main parameters are listed in Table II. Also, the Park transform $P_{n\omega}$ used in this paper is shown in (72), where $n = 1$ for the "Δ" variables and $n = 2$ for "Σ" variables

$$P_{n\omega} = \frac{2}{3} \begin{bmatrix} \cos(n\omega t) & \cos\left(n\omega t - \dfrac{2\pi}{3}\right) & \cos\left(n\omega t - \dfrac{4\pi}{3}\right) \\ \sin(n\omega t) & \sin\left(n\omega t - \dfrac{2\pi}{3}\right) & \sin\left(n\omega t - \dfrac{4\pi}{3}\right) \\ \dfrac{1}{2} & \dfrac{1}{2} & \dfrac{1}{2} \end{bmatrix}.$$
(72)

REFERENCES

[1] A. Lesnicar and R. Marquardt, "An innovative modular multilevel converter topology suitable for a wide power range," in *Proc. IEEE Bologna Power Tech Conf.*, vol. 3. Jun. 2003, p. 6.

[2] R. Adapa, "High-wire act: HVdc technology: The state of the art," *IEEE Power Energy Mag.*, vol. 10, no. 6, pp. 18–29, Nov./Dec. 2012.

[3] A. Antonopoulos, L. Ängquist, and H.-P. Nee, "On dynamics and voltage control of the modular multilevel converter," in *Proc. 13th Eur. Conf. Power Electron. Appl.*, Sep. 2009, pp. 1–10.

[4] L. Harnefors, A. Antonopoulos, S. Norrga, L. Ängquist, and H.-P. Nee, "Dynamic analysis of modular multilevel converters," *IEEE Trans. Ind. Electron.*, vol. 60, no. 7, pp. 2526–2537, Jul. 2013.

[5] S. Rohner, J. Weber, and S. Bernet, "Continuous model of modular multilevel converter with experimental verification," in *Proc. IEEE Energy Convers. Congr. Expo.*, Sep. 2011, pp. 4021–4028.

[6] P. Delarue, F. Gruson, and X. Guillaud, "Energetic macroscopic representation and inversion based control of a modular multilevel converter," in *Proc. 15th Eur. Conf. Power Electron. Appl. (EPE)*, Sep. 2013, pp. 1–10.

[7] H. Saad, X. Guillaud, J. Mahseredjian, S. Dennetière, and S. Nguefeu, "MMC capacitor voltage decoupling and balancing controls," *IEEE Trans. Power Del.*, vol. 30, no. 2, pp. 704–712, Apr. 2015.

[8] H. K. Khalil, *Nonlinear Systems*. Upper Saddle River, NJ, USA: Prentice-Hall, 1996.

[9] J. Wang, R. Burgos, and D. Boroyevich, "Switching-cycle state-space modeling and control of the modular multilevel converter," *IEEE J. Emerg. Sel. Topics Power Electron.*, vol. 2, no. 4, pp. 1159–1170, Dec. 2014.

[10] A. Rasic, U. Krebs, H. Leu, and G. Herold, "Optimization of the modular multilevel converters performance using the second harmonic of the module current," in *Proc. 13th Eur. Conf. Power Electron. Appl.*, Sep. 2009, pp. 1–10.

[11] P. Münch, S. Liu, and G. Ebner, "Multivariable current control of Modular Multilevel Converters with disturbance rejection and harmonics compensation," in *Proc. IEEE Int. Conf. Control Appl.*, Sep. 2010, pp. 196–201.

[12] E. Rakhshani, A. Mir Cantarellas, D. Remon, P. Rodriguez, and I. Candela, "Modeling and control of multi modular converters using optimal LQR controller with integral action," in *Proc. IEEE Energy Convers. Congr. Expo.*, Sep. 2013, pp. 3965–3970.

[13] A. Christe and D. Dujić, "State-space modeling of modular multilevel converters including line frequency transformer," in *Proc. 17th Eur. Conf. Power Electron. Appl. (EPE ECCE-Eur.)*, Sep. 2015, pp. 1–10.

[14] M. Vatani, M. Hovd, and M. Saeedifard, "Control of the modular multilevel converter based on a discrete-time bilinear model using the sum of squares decomposition method," *IEEE Trans. Power Del.*, vol. 30, no. 5, pp. 2179–2188, Oct. 2015.

[15] P. Münch, S. Liu, and M. Dommaschk, "Modeling and current control of modular multilevel converters considering actuator and sensor delays," in *Proc. 35th Annu. Conf. IEEE Ind. Electron.*, Nov. 2009, pp. 1633–1638.

[16] P. Münch, D. Görges, M. Izàk, and S. Liu, "Integrated current control, energy control and energy balancing of modular multilevel converters," in *Proc. 36th Annu. Conf. IEEE Ind. Electron. Soc. (IECON)*, Nov. 2010, pp. 150–155.

[17] K. Ilves, A. Antonopoulos, S. Norrga, and H.-P. Nee, "Steady-state analysis of interaction between harmonic components of arm and line quantities of modular multilevel converters," *IEEE Trans. Power Electron.*, vol. 27, no. 1, pp. 57–68, Jan. 2012.

[18] N. R. Chaudhuri, R. Majumder, B. Chaudhuri, and J. Pan, "Stability analysis of VSC MTDC grids connected to multimachine AC systems," *IEEE Trans. Power Del.*, vol. 26, no. 4, pp. 2274–2784, Oct. 2011.

[19] G. O. Kalcon, G. P. Adam, O. Anaya-Lara, S. Lo, and K. Uhlen, "Small-signal stability analysis of multi-terminal VSC-based DC transmission systems," *IEEE Trans. Power Syst.*, vol. 27, no. 4, pp. 1818–1830, Nov. 2012.

[20] J. Beerten, S. D'Arco, and J. A. Suul, "Identification and small-signal analysis of interaction modes in VSC MTDC systems," *IEEE Trans. Power Del.*, vol. 31, no. 2, pp. 888–897, Apr. 2016.

[21] N. R. Chaudhuri, R. Oliveira, and A. Yazdani, "Stability analysis of vector-controlled modular multilevel converters in linear time-periodic framework," *IEEE Trans. Power Electron.*, vol. 31, no. 7, pp. 5255–5269, Jul. 2016.

[22] P. Kundur, *Power System Stability and Control*. New York, NY, USA: McGraw-Hill, 1994.

[23] S. Liu, Z. Xu, W. Hua, G. Tang, and Y. Xue, "Electromechanical transient modeling of modular multilevel converter based multi-terminal HVDC systems," *IEEE Trans. Power Syst.*, vol. 29, no. 1, pp. 72–83, Jan. 2014.

[24] D. C. Ludois and G. Venkataramanan, "Simplified terminal behavioral model for a modular multilevel converter," *IEEE Trans. Power Electron.*, vol. 29, no. 4, pp. 1622–1631, Apr. 2014.

[25] N.-T. Trinh, M. Zeller, K. Wuerflinger, and I. Erlich, "Generic model of MMC-VSC-HVDC for interaction study with AC power system," *IEEE Trans. Power Syst.*, vol. 31, no. 1, pp. 27–34, Jan. 2016.

[26] G. Bergna-Diaz, J. A. Suul, and S. D'Arco, "Small-signal state-space modeling of modular multilevel converters for system stability analysis," in *Proc. IEEE Energy Convers. Congr. Expo. (ECCE)*, Sep. 2015, pp. 5822–5829.

[27] J. Freytes, L. Papangelis, H. Saad, P. Rault, T. van Cutsem, and X. Guillaud, "On the modeling of MMC for use in large scale dynamic simulations," in *Proc. Power Syst. Comput. Conf. (PSCC)*, Jun. 2016, pp. 1–7.

[28] A. A. J. Far and D. Jovcic, "Circulating current suppression control dynamics and impact on MMC converter dynamics," in *Proc. IEEE Eindhoven PowerTech*, Jun. 2015, pp. 1–6.

[29] A. Jamshidifar and D. Jovcic, "Small-signal dynamic DQ model of modular multilevel converter for system studies," *IEEE Trans. Power Del.*, vol. 31, no. 1, pp. 191–199, Feb. 2016.

[30] V. Najmi, M. N. Nazir, and R. Burgos, "A new modeling approach for modular multilevel converter (MMC) in D-Q frame," in *Proc. IEEE Appl. Power Electron. Conf. Expo. (APEC)*, Mar. 2015, pp. 2710–2717.

[31] G. Bergna, J. A. Suul, and S. D'Arco, "State-space modelling of modular multilevel converters for constant variables in steady-state," in *Proc. IEEE 17th Workshop Control Modeling Power Electron. (COMPEL)*, Jun. 2016, pp. 1–9.

[32] T. Li, A. M. Gole, and C. Zhao, "Harmonic instability in MMC-HVDC converters resulting from internal dynamics," *IEEE Trans. Power Del.*, vol. 31, no. 4, pp. 1738–1747, Aug. 2016.

[33] Q. Tu, Z. Xu, and L. Xu, "Reduced switching-frequency modulation and circulating current suppression for modular multilevel converters," in *Proc. IEEE PES Transmiss. Distrib. Conf. Expo. (T&D)*, May 2012, p. 1.

[34] M. Perez, R. Ortega, and J. Espinoza, "Passivity-based PI control of switched power converters," in *Proc. Eur. Control Conf. (ECC)*, Sep. 2003, pp. 542–547.

[35] M. Hernandez-Gomez, R. Ortega, F. Lamnabhi-Lagarrigue, and G. Escobar, "Adaptive PI stabilization of switched power converters," *IEEE Trans. Control Syst. Technol.*, vol. 18, no. 3, pp. 688–698, May 2010.

[36] G. Bergna-Diaz, D. Zonetti, S. Sanchez, E. Tedeschi, and R. Ortega, "PI passivity-based control of modular multilevel converters for multi-terminal HVDC systems," in *Proc. IEEE 18th Workshop Control Modeling Power Electron. (COMPEL)*, Jul. 2017, pp. 1–8.

[37] J. A. Houldsworth and D. A. Grant, "The use of harmonic distortion to increase the output voltage of a three-phase PWM inverter," *IEEE Trans. Ind. Appl.*, vol. IA-20, no. 5, pp. 1224–1228, Sep. 1984.

[38] S. Norrga, L. Ängquist, and K. Ilves, "Operating region extension for multilevel converters in HVDC applications by optimisation methods," in *Proc. 10th IET Int. Conf. AC DC Power Transmiss. (ACDC)*, Dec. 2012, pp. 1–6.

[39] J. Freytes, G. Bergna, J. A. Suul, S. D'Arco, H. Saad, and X. Guillaud, "State-space modelling with steady-state time invariant representation of energy based controllers for modular multilevel converters," in *Proc. IEEE Manchester PowerTech*, Jun. 2017, pp. 1–7.

[40] H. Saad *et al.*, "Modular multilevel converter models for electromagnetic transients," *IEEE Trans. Power Del.*, vol. 29, no. 3, pp. 1481–1489, Jun. 2014.

[41] R. Teodorescu, M. Liserre, and P. Rodríguez, *Grid Converters for Photovoltaic and Wind Power Systems*, vol. 29. Hoboken, NJ, USA: Wiley, 2011.

[42] J. Freytes *et al.*, "Improving small-signal stability of an MMC with CCSC by control of the internally stored energy," *IEEE Trans. Power Del.*, vol. 33, no. 1, pp. 429–439, Feb. 2018.

[43] G. Bergna-Diaz, J. A. Suul, and S. D'Arco, "Energy-based state-space representation of modular multilevel converters with a constant equilibrium point in steady-state operation," *IEEE Trans. Power Electron.*, vol. 33, no. 6, pp. 4832–4851, Jun. 2018.

[44] X. Wang, Y. Song, and M. Irving, "Modern power systems analysis," in *Small-Signal Stability Analysis of Power Systems*. Boston, MA, USA: Springer, 2008, ch. 8, pp. 489–542.

Julian Freytes received the Electrical Engineering degree from the Universidad Nacional del Sur, Bahía Blanca, Argentina, in 2013, the M.Sc. degree in electrical engineering for sustainable development from the Université des Sciences et Technologies de Lille, Villeneuve-d'Ascq, France, in 2014, and the Ph.D. degree in small-signal stability analysis of modular multilevel converters and application to MMC-based multiterminal dc grids from the École Centrale de Lille, Villeneuve-d'Ascq, in 2017.

He is currently with GE Power, Massy, France. His current research interests include the modeling and control of power electronics for HVDC systems.

Xavier Guillaud (M'04) received the M.Sc. and Ph.D. degrees in electrical engineering from the University of Lille, Villeneuve-d'Ascq, France, in 1988 and 1992, respectively.

Since 2002, he has been a Professor with L2EP, University of Lille, where he was involved in the modeling and control of power electronic systems. He has also studied the integration of distributed generation and especially renewable energy in power systems. He is currently leading the development of an experimental facility composed of actual power electronic converters interacting with virtual grids modeled in a real-time simulator. He is also involved in several European Union projects about power electronics in the grid and different projects with French companies. His current research interest includes high-voltage power electronic converters in transmission systems.

He is a member of the Technical Program Committee of the Power System Computation Conference and an Associated Editor of Sustainable Energy, Grids, and Networks.

Salvatore D'Arco received the M.Sc. and Ph.D. degrees in electrical engineering from the University of Naples Federico II, Naples, Italy, in 2002 and 2005, respectively.

From 2006 to 2007, he was a Post-Doctoral Researcher with the University of South Carolina, Columbia, SC, USA. In 2008, he joined ASML, Veldhoven, The Netherlands, as a Power Electronics Designer. From 2010 to 2012, he was a Post-Doctoral Researcher with the Department of Electric Power Engineering, Norwegian University of Science and Technology, Trondheim, Norway. In 2012, he joined SINTEF Energy Research, Trondheim, where he is currently a Senior Research Scientist. His current research interests include control and analysis of power-electronic conversion systems for power system applications, especially real-time simulation and rapid prototyping of converter control systems.

Gilbert Bergna-Diaz received the Electrical Power Engineering degree from the Universidad Simón Bolívar, Caracas, Venezuela, in 2008, the Research Master degree in electrical energy from the École Supérieure d'Électricité (Supélec), Paris, France, in 2010, and the joint Ph.D. degree in electric power engineering from École CentraleSupélec, Paris, and the Norwegian University of Science and Technology (NTNU), Trondheim, Norway, in 2015.

In 2014, he joined SINTEF Energy Research, Trondheim, as a Research Scientist, where he was involved in modeling, analysis, and control of HVDC transmission systems. Since 2016, he has been a Post-Doctoral Research Fellow at NTNU, where he is involved in (port-Hamiltonian) energy modeling and nonlinear (passivity-based) control of multi-terminal HVDC grids.

Jon Are Suul (M'11) received the M.Sc. degree in energy and environmental engineering and the Ph.D. degree in electric power engineering from the Norwegian University of Science and Technology (NTNU), Trondheim, Norway, in 2006 and 2012, respectively.

From 2006 to 2007, he was with SINTEF Energy Research, Trondheim, where he was involved in the simulation of power electronic converters and marine propulsion systems. Since 2012, he has been a Research Scientist with SINTEF Energy Research, and in the period from 2012 to 2016 he was also a part-time Post-Doctoral Researcher with the Department of Electric Power Engineering, NTNU until 2016. Since 2017, he has been an Adjunct Associate Professor with the Department of Engineering Cybernetic, NTNU. His current research interests include modeling, analysis, and control of power electronic converters in power systems, renewable energy applications and for electrification of transport.